Ciesielski, P. F., Kristoffersen, Y., et al., 1991
Proceedings of the Ocean Drilling Program, Scientific Results, Vol. 114

24. FINE-FRACTION CARBONATE OXYGEN AND CARBON ISOTOPE RESULTS FROM SITE 704: IMPLICATIONS FOR MOVEMENT OF THE POLAR FRONT DURING THE LATE PLIOCENE[1]

Gregory A. Mead,[2] David A. Hodell,[2] Daniel W. Müller,[3] and Paul F. Ciesielski[2]

ABSTRACT

Ocean Drilling Program Site 704 in the subantarctic South Atlantic was drilled to investigate the response of the Southern Ocean to climatic and oceanographic developments during the late Neogene.

Stable oxygen and carbon isotopes of fine-fraction (<63 μm) carbonate were analyzed to supplement similar analyses of benthic and planktonic foraminifers. The fine fraction is generally composed primarily of coccoliths, and isotopic analyses of the fine fraction were made to complement the foraminiferal analyses. The isotopic curves thus generated suggest paleoceanographic changes not recognizable by the use of benthic and planktonic foraminifers alone.

The global Chron 6 carbon isotope shift, found at 253–244 mbsf (6.39–6.0 Ma) at Site 704 in the planktonic and benthic record, is seen in the fine-fraction $\delta^{13}C$ record as a gradual decrease from 255 mbsf (6.44 Ma) to 210 mbsf (4.24 Ma).

At 170 mbsf, mean $\delta^{18}O$ values of *Neogloboquadrina pachyderma* increase by 0.6‰–0.7‰ (Hodell and Ciesielski, this volume), reflecting decreased temperature and increased continental ice volume. Accumulation rates increase by 3.3 times above this depth (which corresponds to an age of 2.5 Ma), suggesting increased upwelling and biologic productivity.

Carbon isotopic values of fine-fraction carbonate decrease by about 1.5‰ at 2.6 Ma; however, no change is recorded in the $\delta^{13}C$ of *N. pachyderma*. The fine-fraction $\delta^{13}C$ shift slightly precedes an average 1‰ decrease in $\delta^{13}C$ in benthic foraminifers. The cause of the benthic $\delta^{13}C$ shift (most likely due to a change in deep water circulation; Hodell and Ciesielski, this volume) is probably not directly related to the fine-fraction shift. The fine-fraction shift is most likely caused by (1) a change in the upwelling to productivity ratio at this site, with increased upwelling bringing lighter carbon to surface waters, more productivity, and higher sedimentation rates and (2) a change in the particle composition of the fine fraction. The increased upwelling is probably due to a northward migration of the Antarctic Polar Front to a position nearer Site 704.

INTRODUCTION

Ocean Drilling Program (ODP) Site 704 was drilled on the Meteor Rise at 46°53′S, 7°25′E, at a depth of 2532 m (Fig. 1). The site is just north of the present position of the Antarctic Polar Front Zone (APFZ), and south of the Subtropical Convergence, as defined by the expendable bathythermograph data of Lutjeharms (1985). Site 704 recovered a nearly continuous section from the middle Miocene through the latest Pleistocene using hydraulic piston corer and extended core barrel coring techniques in two adjacent holes, with carbonate content ranging from 0% to 96%. Paleomagnetic and biostratigraphic analyses show that the only gap in the Pliocene-Pleistocene section is a possible compressed interval in the Brunhes. The upper 50 m of section is slightly to severely disturbed, however, so the age of this interval is not well constrained. Carbon and oxygen isotope analyses of planktonic and benthic foraminifers (see Hodell et al., this volume; Müller et al., this volume) and the bulk fine fraction (>63 μm) have been used to examine paleoceanographic conditions in the South Atlantic during the late Neogene.

The history of climatic change through the Cenozoic has been characterized by periods of relative stasis punctuated by sudden episodes of change (Shackleton and Kennett, 1975). These events are recorded in oxygen and carbon isotopic records from the deep sea and can help us understand the causes and effects of these changes.

The Neogene was the time during which major, permanent ice caps developed and during which the present glacial-interglacial cycles were initiated in the Northern Hemisphere. Although small valley glaciers or temporary ice caps may have occurred on Antarctica during the Oligocene (Shackleton and Kennett, 1975; Matthews and Poore, 1980; Miller and Fairbanks, 1983; Miller et al., 1985), a permanent ice cap on East Antarctica did not develop until the mid-Miocene, at about 14 Ma (Shackleton and Kennett, 1975). Deep Sea Drilling Project (DSDP) drilling at several sites in the North Atlantic has provided evidence that significant Northern Hemisphere glaciation began in the late Pliocene (Shackleton et al., 1984; Raymo et al., 1989). Shackleton et al. (1984) first presented evidence that ice-rafted debris began to accumulate in the North Atlantic at DSDP Site 552 at about 2.4 Ma, while carbonate concentration in the sediment decreased due to the diluent effect of ice-rafted debris. In addition, isotopic analyses of benthic foraminifers revealed an average ^{18}O enrichment in biogenic calcite of over 1.0‰, indicating the accumulation of isotopically light continental ice. The initial glacial episodes resulted in oxygen isotope fluctuations of about 1‰, at periods of approximately 41,000 yr, corresponding to Milankovitch obliquity variation (Ruddiman et al., 1986). Raymo et al. (1989) found small amounts of ice-rafted debris present in sediments as old as 2.65 Ma in DSDP Hole 607. Spectral analysis of oxygen isotopic variations of Pliocene sediments from Hole 607 also indicates periodicities of about 41,000 yr, although with a lower amplitude than after 2.4 Ma. By the Brunes/Matuyama boundary, the amplitude of the $\delta^{18}O$ variations had increased to about 2‰, and the dominant

[1] Ciesielski, P. F., Kristoffersen, Y., et al., 1991. *Proc. ODP, Sci. Results*, 114: College Station, TX (Ocean Drilling Program).
[2] Department of Geology, University of Florida, Gainesville, FL 32611.
[3] Geologisches Institut, ETH-Zentrum, CH-8092 Zürich, Switzerland.

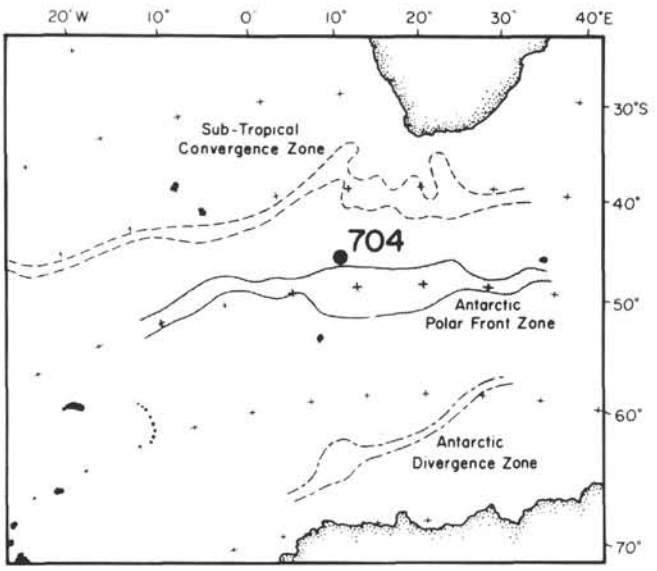

Figure 1. The position of ODP Site 704 in the eastern subantarctic South Atlantic relative to the major hydrographic fronts (modified after Lutjeharms, 1985).

period of the glacial-interglacial cycles increased to approximately 100,000 yr (Shackleton et al., 1984; Ruddiman et al., 1986, 1989).

The onset of large-scale Northern Hemisphere glaciation is a key event in the development of the Earth's present climatic regime, with cyclic glaciations characterizing the Earth's climate during the Pleistocene and late Pliocene. However, the interaction of the Southern Hemisphere with the Northern Hemisphere at the onset of these glaciations is not well understood.

Stable Isotopic Studies of Fine-Fraction Carbonate

Several studies have examined the utility of calcareous nannofossil isotopic data as paleoceanographic indicators (Anderson and Cole, 1975; Margolis et al., 1975; Goodney et al., 1980; Dudley et al., 1980, 1986; Paull and Theirstein, 1987). Results of these studies have been inconclusive because several variables control the isotopic composition of the fine fraction. Margolis et al. (1975) found that nannofossil $\delta^{18}O$ was roughly equivalent to that of planktonic foraminifers, whereas $\delta^{13}C$ of nannofossil calcite exhibited a variable relationship to planktonic foraminiferal $\delta^{13}C$. Goodney et al. (1980) investigated the isotopic response of calcareous nannofossils in Holocene sediments. They found that $\delta^{18}O$ and $\delta^{13}C$ of the fine fraction covaried, with a slope near 1. They suggested that the trend was caused by assemblage changes in the fine fraction. Paull and Theirstein (1987) found that different grain-size subfractions of the fine fraction from the same sample (roughly corresponding to different taxonomic groups) had different $\delta^{18}O$ and $\delta^{13}C$ values. The isotopic compositions of the subfractions lay along a linear trend of increasing $\delta^{18}O$ with increasing $\delta^{13}C$, similar to that of Goodney et al. (1980).

Another finding of Goodney et al. (1980) was the existence of a latitudinal pattern to the carbon isotopic gradient between planktonic foraminifers and nannofossils. They found that when $\delta^{13}C$ of planktonic foraminifers increased, $\delta^{13}C$ of calcareous nannofossils decreased, increasing the gradient between them, and, in addition, that this effect varied systematically with latitude. They suggested that the mirrored relationship was due to effects of changing rates of productivity on $\delta^{13}C$ of ΣCO_2. In low-productivity areas, photosynthesis would have little effect on $\delta^{13}C$, and the $\delta^{13}C$ values of planktonic foraminifers and the fine fraction would be similar. In areas of high productivity, photosynthesis preferentially extracts ^{12}C, increasing $\delta^{13}C$ and causing the $\delta^{13}C$ of planktonic foraminifers to be elevated relative to that of the fine fraction. Dudley et al. (1980) suggested that because coccolith calcite deposition is intracellular, metabolic CO_2 may be incorporated into the calcite, and Goodney et al. (1980) suggested that nannofossil $\delta^{13}C$ would be lower for that reason.

In the Southern Ocean, conditions controlling $\delta^{13}C$ of surface waters are somewhat different. Insolation in the Antarctic area is less than in more temperate areas because of the low angle of the sun. Furthermore, temperatures are low, slowing biologic processes. Primary productivity in this area is thus light-limited rather than nutrient-limited (Knox and McElroy, 1984). Therefore, surface waters in areas of high productivity in high latitudes tend to be characterized by low $\delta^{13}C$ values because the balance between preferential removal of ^{12}C by photosynthesis and carbon with low $\delta^{13}C$ values supplied by upwelling/mixing will be in shifted toward the supply side. In areas of high productivity caused by increased upwelling, the effect of photosynthesis on $\delta^{13}C$ would be swamped by the upwelling effect. In areas of low productivity caused by slower replenishment of carbon and other nutrients, nearly all carbon would be extracted by photosynthesis, producing greatly enriched $\delta^{13}C$. Carbon isotopic compositions of surface waters thus depend on the balance between the rate of carbon removed because of photosynthesis and the rate of ^{12}C-enriched carbon supplied by upwelling and surface currents.

Because of this balance and other factors discussed subsequently, $\delta^{13}C$ gradients exist in the surface waters of the Antarctic, with lower $\delta^{13}C$ values occurring in the high-productivity area south of the Polar Front (Kroopnick, 1980, 1985). Carbon isotopic composition of surface water is also affected by exchange with the atmosphere. Charles and Fairbanks (1990) have shown that there is a decrease in $\delta^{13}C$ both north and south of the Polar Front. They suggest that these gradients result not only from upwelling/productivity effects but also from the rate of gas exchange and the temperature-dependent nature of the gas exchange fractionation north of the front and from gas exchange fractionation and incomplete equilibration of surface waters with the atmosphere south of the front.

This paper will discuss results of oxygen and carbon isotopic analyses of fine-fraction carbonate samples from ODP Site 704 in the South Atlantic, which suggest that

1. a northward migration of the Antarctic Polar Front over this site occurred shortly before the onset of Northern Hemisphere glaciation, leading to
2. increasing productivity, and
3. a change in the $\delta^{13}C$ of pelagic carbonate at this site.

METHODS

Age-Depth Model

The time scale used in this report is calibrated to the Berggren et al. (1985) time scale. The *S* terminology for paleomagnetic boundaries is from Hailwood (1989). The tie points shown in Table 1 are from Hailwood and Clement (this volume), and other dates were obtained by linear interpolation between these points.

Sampling Strategy

Holes 704A and 704B were both used to construct the isotope section. Samples were used from the upper 25 m of both holes. Core 114-704A-4H was highly disturbed, so sam-

Table 1. Age-depth model from Hailwood and Clement (this volume). The *S* terminology is from Hailwood (1989); dates are from Berggren et al. (1985).

Depth (mbsf)	Age (Ma)	Datum[a]
0.00	0.00	Seafloor
1.14	0.195	LAAD *Hemidiscus karstenii*
15.55	0.62	LAD *Actinocyclus ingens*
34.51	0.73	Brunhes/Matuyama (S1N/S1R) boundary
44.50	0.98	Base Jaramillo
87.40	1.66	Top Olduvai
100.25	1.89	Base Olduvai
168.72	2.47	Matuyama/Gauss (S2R/S3N) boundary
169.13	2.64	LAD *Nitzschia weaveri*
176.70	2.92	Top Kaena
177.98	2.99	Base Kaena
178.96	3.08	Top Mammoth
181.13	3.18	Base Mammoth
186.69	3.40	Gauss/Gilbert (S3N/S3R) boundary
195.79	3.88	Top Cochiti (S3R/S4N boundary)
201.94	3.97	Base Cochiti (S4N.10)
204.19	4.10	Top Nunivak (S4N.25)
210.29	4.24	Base Nunivak (S4N.40)
211.99	4.40	Top C1 (S4N.58)
213.22	4.47	Base C1 (S4N.66)
217.29	4.57	S4N.78
219.44	4.77	S4N/S4R boundary
224.75	5.15	FAD *Thalassiosia oestrupii*
224.89	5.35	S4R/S5N boundary
231.00	5.53	S5N.33
234.00	5.68	S5N.61
241.50	5.89	S5N/S5R boundary
252.20	6.37	S5R.59
257.50	6.50	S5R.75
259.50	6.70	S5R/S6N boundary
264.50	6.78	S6N.11
265.50	6.85	S6N.21
267.50	7.28	S6N.82
270.20	7.35	S6N.92
275.20	7.41	S6N/S6R boundary
290.00	7.90	S6R/S7N boundary
308.50	8.21	S7N.52
309.50	8.41	S7N.85
318.50	8.50	S7N/S7R boundary
324.00	8.71	S7R.50
327.00	8.80	S7R.71
338.50	8.92	S7R/S8N boundary
379.95	10.40	S8N/S8R boundary

[a] LAAD = last absolute appearance datum; LAD = last-appearance datum; FAD = first-appearance datum.

ples from Hole 704B only were used from 25.41 to 34.26 m below seafloor (mbsf). Color variation (Shipboard Scientific Party, 1988) and carbonate content (Froelich et al., this volume) in the upper part of the section show little correlation between the holes. Because of this, no attempt was made to splice samples from the two holes. Instead, the data from each hole are plotted on the figures separately, but on a common depth scale. Sample recovery was low or zero in cores from Hole 704A below Core 114-704A-25X (235.2 mbsf), so samples from Holes 704A and 704B were overlapped from 213.91 to 233.41 mbsf. Carbonate data (Froelich et al., this volume) show a variable offset in depth between the holes of up to 1 m, but no consistent correlation is possible based on these data. Therefore, again, the data are plotted separately on a common depth scale. Samples from Hole 704B were used exclusively from 233.81 mbsf to the deepest fine-fraction sample at 289.66 mbsf, with an age of 7.89 Ma.

The sampling intervals vary with depth. Within the upper 80 m, the sampling interval averages 30.9 cm, or one per 6000 yr. Between 80 and 168 mbsf, the average is 145.8 cm, or one per 15,000 yr. The average sampling interval from 168 to 200 mbsf is about the same, 166.7 cm, but because of a sedimentation rate change, the average sample frequency is only one per 77,500 yr. From 200 to 290 mbsf, the sampling interval is smaller, averaging 37.8 cm, and the sampling frequency averages one per 16,800 yr.

Isotopic Analyses

The fine-fraction (<63 μm) samples of Site 704 were obtained by disaggregating bulk samples in a water solution of warm sodium hexa-metaphosphate and washing through a 63-μm sieve. The coarse fraction was saved for isotopic analyses of foraminifers (Hodell et al., this volume). The fine-fraction residues were collected and settled for at least 24 hr. Excess water was poured off, and the fine-fraction was concentrated by centrifugation and dried in a 50°C oven. Fine-fraction samples were mechanically homogenized, and a small subsample was roasted at 400°C in a vacuum for 1 hr to remove organic carbon. The subsamples were reacted in a common 100% orthophosphoric acid bath at 70°C to release CO_2, which was analyzed in an automated triple collector VG Isogas Prism mass spectrometer. Isotopic results were corrected to PDB via a set of intermediate standards (Hodell et al., 1989). Precision of replicate fine-fraction analyses averaged 0.16°/oo for oxygen and 0.13°/oo for carbon. Isotopic results that differed greatly from the analysis of neighboring samples were reanalyzed for confirmation. If repeat analyses differed by more than 0.5°/oo, a third replicate was analyzed; analyses that differed from the other two by more than 0.5°/oo were rejected, and if all three were within 0.5°/oo, all were accepted.

Barrera and Savin (1987) investigated the effect of isotopic exchange between the fine fraction and evaporating wash water. They found that substantial effects, caused by Rayleigh fractionation, occurred in the very fine fraction (<10 μm) that they analyzed. To investigate whether any similar effects occurred with the Site 704 samples, six fine-fraction samples were resuspended after initial centrifugation, split, and the water replaced with methanol in one of the splits through the use of three successive resuspensions and centrifuge concentrations. The results are shown in Table 2. The oxygen isotopes of the water-dried fraction differ from those of the methanol-dried fraction by an average of 0.01°/oo ± 0.07°/oo (two standard deviations), and carbon isotopes differ by an average of 0.02 ± 0.10°/oo (two standard deviations). We conclude that the samples used in this study were not affected by Rayleigh fractionation during drying.

Analytic precision as established by repeat analyses of an internal working standard (Carrara Marble) is 0.13°/oo for oxygen and 0.04°/oo for carbon isotopes.

Fine-Fraction Compositional Analysis

One objective of this study was to determine whether compositional changes in the fine-fraction assemblage caused changes in the isotopic composition. Portions of the homogenized fine fraction were selected from samples at approximately 10-m intervals. Slides of these samples were used to estimate fine-fraction composition. The method of Moore (1973) was used to make slides with randomly settled grains, to ensure a representative estimate of fine-fraction composition. The percentage of three calcareous particle types (foraminifers, coccoliths, and micrite) was estimated from each slide, with the least common particle type estimated first, and the most common type calculated by the difference between 100% and the sum of the other two particle types.

RESULTS

The fine-fraction carbonate isotope record shows significant variability in both carbon and oxygen isotopes (Fig. 2 and

Table 2. Effects of methanol drying vs. water drying on the isotopic content of the fine fraction.

Core, section, interval (cm)	$\delta^{18}O$ Water dried	$\delta^{18}O$ Methanol dried	$\delta^{18}O$ Difference between methods	$\delta^{13}C$ Water dried	$\delta^{13}C$ Methanol dried	$\delta^{13}C$ Difference between methods
114-704A-						
19X-2, 21	2.92	2.89	0.03	0.92	0.88	0.04
19X-4, 21	2.54	2.57	−0.03	0.45	0.51	−0.06
20X-2, 21	2.58	2.55	0.03	0.54	0.59	−0.05
20X-6, 21	2.16	2.10	0.06	0.51	0.60	−0.09
21X-2, 46	2.06	2.09	−0.03	0.44	0.44	0.00
22X-2, 21	2.24	2.23	0.01	0.76	0.73	0.03
Mean			0.01			−0.02

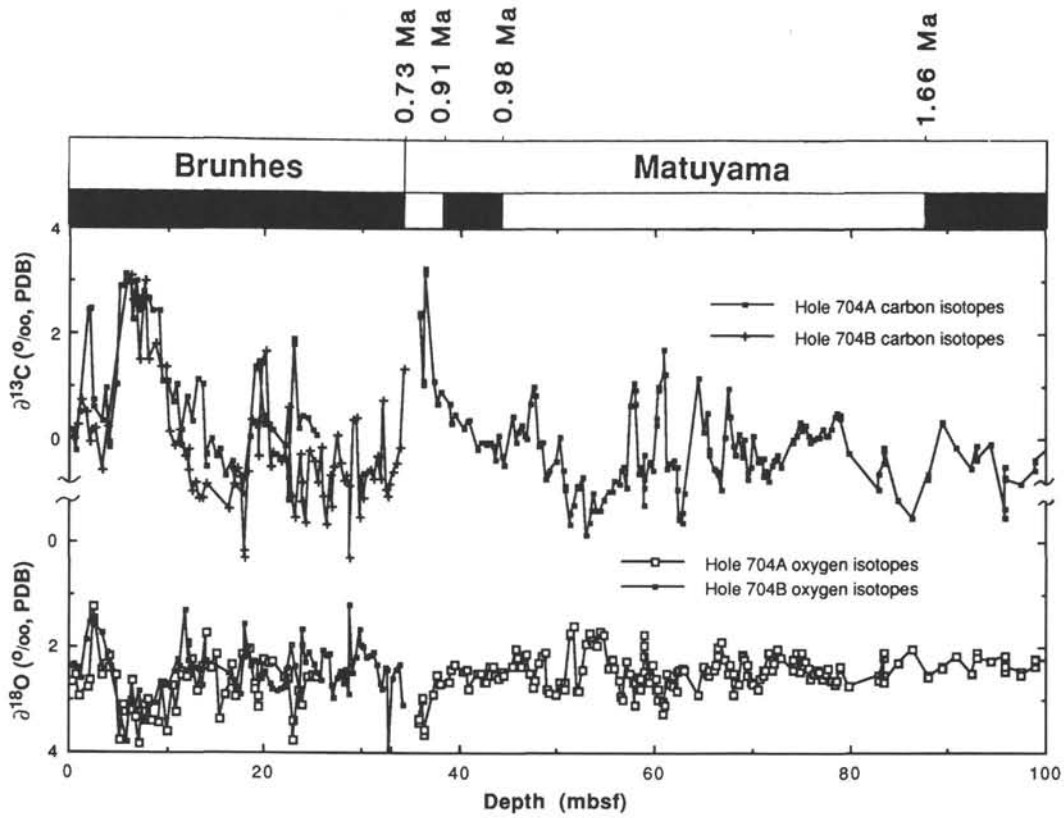

Figure 2. Fine-fraction $\delta^{13}C$ and $\delta^{18}O$ records vs. depth, 0–300 mbsf.

Table 3). The maximum amplitude in both isotope signals occurs in the upper 40 m, with a range of 5.53°/oo (−2.3°/oo to 3.23°/oo) for $\delta^{13}C$ and 2.77°/oo (1.18°/oo to 3.95°/oo) for $\delta^{18}O$.

Covariance between $\delta^{13}C$ and $\delta^{18}O$ occurs over much of the fine-fraction record (Fig. 3). These results contrast with the trend line found by Goodney et al. (1980) of much stronger covariance between $\delta^{13}C$ and $\delta^{18}O$ in the tops of cores from the Indian Ocean. However, it is important to remember that the core-top data of Goodney et al. (1980) were not affected by ice volume changes, whereas downcore data will be. Simultaneous maxima in $\delta^{13}C$ and $\delta^{18}O$ occur at several levels: 238.9–240.4 mbsf (5.8 Ma), 221.2 mbsf (4.90 Ma), 203.5 mbsf (4.06 Ma), 187.4 mbsf (3.44 Ma), 181.4 mbsf (3.19 Ma), and 175 mbsf (2.86 Ma).

Note that the data from Holes 704A and 704B correspond very well in the areas of overlap (0–36.2 and 213.9–233.4 mbsf) even without splicing. This suggests that little displacement of sediment has occurred in the disturbed upper section. The isotopic signal is small in the lower region of overlap, and thus little difference in values is seen there despite the variable 1-m offset previously mentioned.

Oxygen Isotopes

The $\delta^{18}O$ record exhibits less variability than the $\delta^{13}C$ record (Fig. 2). From about 290 mbsf (7.9 Ma) to 264–253 mbsf (6.77–6.39 Ma), the oxygen isotopic composition of the fine fraction became gradually more enriched in ^{18}O, from an average of 2.44°/oo between 290 and 280 mbsf to an average of 2.82°/oo between 264 and 253 mbsf. At this point, $\delta^{18}O$ began to decrease over the next 40 m (1.7 m.y.), to about 2°/oo at 222 mbsf (4.95 Ma). There is one short period of enrichment in ^{18}O at about 240 mbsf (5.85 Ma), with $\delta^{18}O$ increasing to more than 3°/oo. From 222 to about 180 mbsf (3.13 Ma), a slow, uneven $\delta^{18}O$ enrichment occurs, rising from about 2°/oo to about

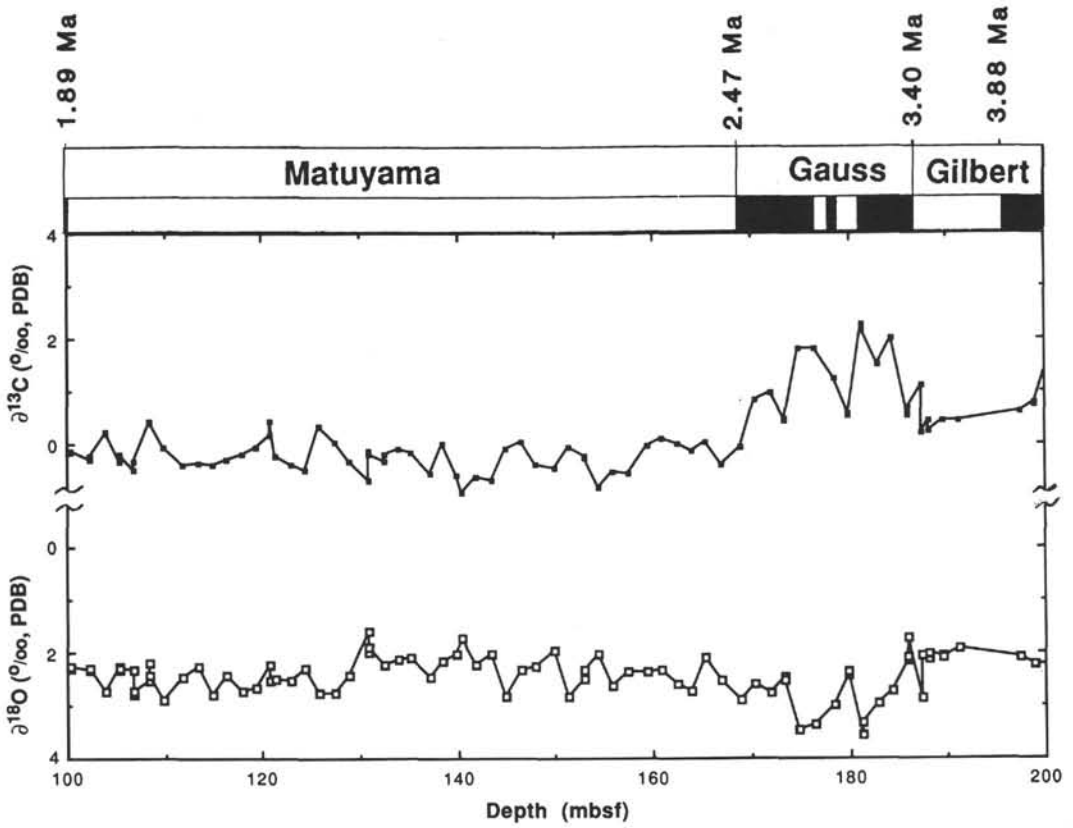

Figure 2 (continued).

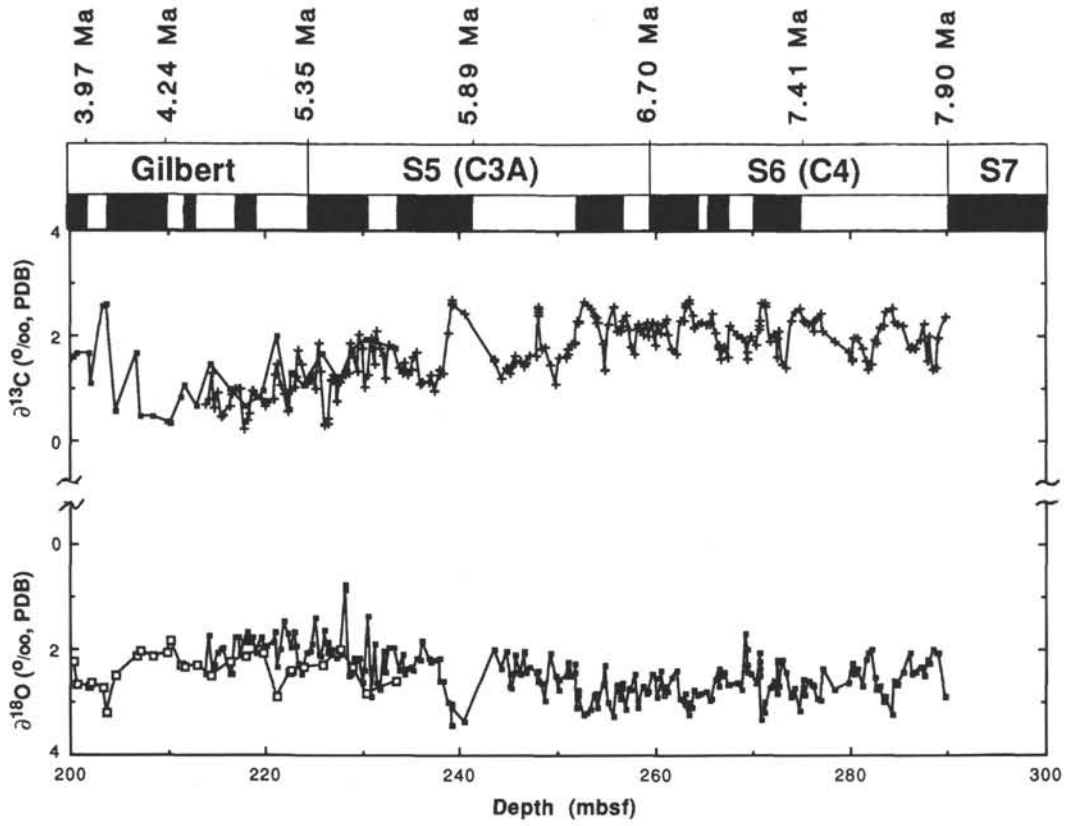

Figure 2 (continued).

Table 3. Fine-fraction $\delta^{13}C$ and $\delta^{18}O$ values, Site 704.

Core, section, interval (cm)	Depth (mbsf)	Age (Ma)	$\delta^{13}C$	$\delta^{18}O$
114-704A-				
1H-1, 41	0.41	0.0701	0.158	2.678
1H-1, 78	0.78	0.1334	−0.236	2.516
1H-1, 110	1.10	0.1882	0.486	2.939
1H-2, 41	1.91	0.2177	2.432	2.750
1H-2, 78	2.22	0.2269	2.473	2.637
1H-2, 110	2.60	0.2381	0.573	1.223
1H-2, 110	2.60	0.2381	0.720	1.461
1H-3, 41	3.41	0.2620	0.333	2.545
1H-3, 41	3.41	0.2620	0.337	2.427
1H-3, 78	3.78	0.2729	0.950	2.321
1H-3, 78	3.78	0.2729	0.950	2.321
1H-3, 110	4.10	0.2823	−0.087	2.166
1H-3, 110	4.10	0.2823	−0.192	2.382
1H-4, 41	4.91	0.3062	1.015	2.536
1H-4, 78	5.28	0.3171	2.907	3.769
1H-4, 110	5.60	0.3265	2.897	3.108
1H-4, 125	5.75	0.3310	3.138	3.224
1H-5, 21	6.21	0.3445	2.970	3.201
1H-5, 41	6.41	0.3504	2.263	2.620
1H-5, 78	6.78	0.3613	3.010	3.324
1H-5, 110	7.10	0.3708	2.434	3.838
2H-1, 41	7.61	0.3858	2.801	3.097
2H-1, 82	8.02	0.3979	2.652	2.990
2H-1, 132	8.52	0.4127	2.423	3.404
2H-2, 41	9.11	0.4301	2.437	3.436
2H-2, 82	9.52	0.4422	1.106	2.682
2H-2, 132	10.02	0.4569	1.075	3.588
2H-3, 41	10.61	0.4743	0.677	2.742
2H-3, 82	11.02	0.4864	1.025	3.221
2H-3, 132	11.52	0.5011	0.166	2.528
2H-3, 132	11.52	0.5011	−0.154	2.445
2H-4, 41	12.11	0.5185	0.787	2.573
2H-4, 82	12.52	0.5306	0.317	2.224
2H-4, 132	13.02	0.5454	1.120	2.822
2H-5, 41	13.61	0.5628	1.017	2.365
2H-5, 82	14.02	0.5749	−0.314	2.364
2H-5, 82	14.02	0.5749	−0.555	1.735
2H-5, 132	14.52	0.5896	−0.021	2.406
2H-6, 42	15.12	0.6073	−0.354	2.124
2H-6, 82	15.52	0.6191	−0.212	3.352
2H-6, 132	16.02	0.6227	−0.716	2.903
2H-7, 41	16.61	0.6262	−0.435	2.668
2H-7, 41	16.61	0.6262	−0.595	2.331
3H-1, 28	16.98	0.6283	−0.912	2.924
3H-1, 116	17.86	0.6334	−1.084	2.115
3H-2, 28	18.48	0.6370	0.025	2.037
3H-2, 81	19.01	0.6401	1.322	2.783
3H-2, 81	19.01	0.6401	1.348	2.689
3H-2, 116	19.36	0.6421	1.392	2.921
3H-2, 116	19.36	0.6421	1.459	3.146
3H-3, 28	19.98	0.6457	0.262	2.261
3H-3, 28	19.98	0.6457	0.301	2.238
3H-3, 28	19.98	0.6457	0.427	2.254
3H-3, 82	20.52	0.6488	0.252	2.302
3H-3, 116	20.86	0.6508	0.146	2.265
3H-4, 82	22.02	0.6575	−0.161	2.554
3H-4, 116	22.36	0.6595	−0.756	2.609
3H-4, 116	22.36	0.6595	−1.193	2.455
3H-5, 28	22.98	0.6631	1.783	3.405
3H-5, 28	22.98	0.6631	1.909	3.774
3H-5, 82	23.52	0.6662	0.179	2.820
3H-5, 116	23.86	0.6682	0.431	3.095
3H-6, 28	24.48	0.6718	0.400	2.550
3H-6, 82	25.02	0.6749	0.156	2.524
3H-6, 116	25.36	0.6769	0.053	2.561
5H-1, 21	35.91	0.7650	2.396	3.354
5H-1, 21	35.91	0.7650	2.328	3.443
5H-1, 51	36.21	0.7725	1.030	2.953
5H-1, 51	36.21	0.7725	1.080	3.006
5H-1, 81	36.51	0.7801	3.226	3.668
5H-1, 81	36.51	0.7801	3.121	3.551
5H-2, 21	37.41	0.8026	1.103	2.893
5H-2, 51	37.71	0.8101	0.657	2.518
5H-2, 81	38.01	0.8176	0.891	2.702
5H-3, 21	38.91	0.8401	0.671	2.649

Table 3 (continued).

Core, section, interval (cm)	Depth (mbsf)	Age (Ma)	$\delta^{13}C$	$\delta^{18}O$
5H-3, 51	39.21	0.8476	0.285	2.417
5H-3, 81	39.51	0.8551	0.457	2.316
5H-4, 21	40.41	0.8777	0.178	2.462
5H-4, 51	40.71	0.8852	0.330	2.444
5H-4, 82	41.02	0.8929	0.355	2.781
5H-5, 21	41.91	0.9152	−0.203	2.480
5H-5, 51	42.21	0.9227	−0.074	2.485
5H-5, 82	42.52	0.9305	−0.089	2.649
5H-5, 111	42.81	0.9377	−0.123	2.662
5H-5, 141	43.11	0.9452	−0.096	2.367
5H-6, 21	43.41	0.9527	−0.157	2.358
5H-6, 51	43.71	0.9602	−0.408	2.538
5H-6, 81	44.01	0.9677	0.043	2.606
5H-6, 111	44.31	0.9753	−0.362	2.465
5H-6, 141	44.61	0.9817	−0.506	2.543
6H-1, 20	45.40	0.9943	0.419	2.370
6H-1, 55	45.75	0.9998	−0.087	2.015
6H-1, 85	46.05	1.0046	0.137	2.185
6H-1, 106	46.26	1.0079	0.248	2.349
6H-1, 141	46.61	1.0135	0.049	2.161
6H-2, 20	46.90	1.0180	−0.010	2.119
6H-2, 55	47.25	1.0236	0.645	2.510
6H-2, 85	47.55	1.0283	1.003	2.754
6H-2, 106	47.76	1.0317	0.807	2.614
6H-2, 141	48.11	1.0372	−0.150	2.299
6H-3, 20	48.40	1.0418	−0.091	2.159
6H-3, 55	48.75	1.0474	−0.788	2.103
6H-3, 85	49.05	1.0521	−0.696	2.783
6H-3, 105	49.25	1.0553	−0.602	2.878
6H-4, 20	49.90	1.0656	−0.438	2.891
6H-4, 55	50.25	1.0711	0.034	2.676
6H-4, 85	50.55	1.0759	−0.615	2.777
6H-4, 106	50.76	1.0792	−0.908	2.788
6H-4, 106	50.76	1.0792	−0.971	2.677
6H-5, 20	51.40	1.0894	−1.651	1.747
6H-5, 20	51.40	1.0894	−1.452	1.735
6H-5, 55	51.75	1.0949	−1.279	1.581
6H-5, 85	52.05	1.0997	−0.917	2.815
6H-5, 106	52.26	1.1030	−0.947	2.846
6H-5, 141	52.61	1.1086	−0.748	2.436
6H-6, 20	52.90	1.1132	−1.843	1.942
6H-6, 55	53.25	1.1187	−1.604	1.739
6H-6, 85	53.55	1.1235	−1.369	1.847
6H-6, 106	53.76	1.1268	−1.044	1.928
6H-6, 141	54.11	1.1323	−1.384	1.969
6H-7, 20	54.40	1.1369	−1.386	1.682
6H-7, 55	54.75	1.1425	−1.169	1.770
7H-1, 60	55.30	1.1512	−1.013	2.380
7H-1, 91	55.61	1.1561	−1.021	2.222
7H-1, 120	55.90	1.1607	−0.814	2.389
7H-2, 11	56.31	1.1672	−0.883	2.619
7H-2, 30	56.50	1.1702	−0.624	2.924
7H-2, 60	56.80	1.1750	−0.550	3.003
7H-2, 91	57.11	1.1799	−0.964	2.260
7H-2, 120	57.40	1.1845	0.617	2.502
7H-3, 11	57.81	1.1910	1.058	2.669
7H-3, 30	58.00	1.1940	0.910	3.081
7H-3, 30	58.00	1.1940	0.665	2.649
7H-3, 60	58.30	1.1987	−0.682	2.549
7H-3, 91	58.61	1.2037	−0.562	2.600
7H-3, 91	58.61	1.2037	−0.633	2.797
7H-3, 91	58.61	1.2037	−0.602	2.769
7H-3, 120	58.90	1.2083	−0.303	1.752
7H-3, 120	58.90	1.2083	−0.958	1.948
7H-3, 120	58.90	1.2083	−0.788	2.446
7H-3, 120	58.90	1.2083	−1.275	2.176
7H-4, 30	59.50	1.2178	−0.480	2.578
7H-4, 30	59.50	1.2178	−0.461	2.669
7H-4, 60	59.80	1.2225	−0.632	2.331
7H-4, 91	60.11	1.2274	0.397	2.595
7H-4, 91	60.11	1.2274	0.240	2.797
7H-4, 120	60.40	1.2320	0.911	2.998
7H-4, 120	60.40	1.2320	0.978	2.782
7H-5, 11	60.81	1.2385	1.707	3.275
7H-5, 11	60.81	1.2385	1.226	3.028
7H-5, 30	61.00	1.2415	1.232	3.100
7H-5, 60	61.30	1.2463	−0.575	2.505

Table 3 (continued).

Core, section, interval (cm)	Depth (mbsf)	Age (Ma)	$\delta^{13}C$	$\delta^{18}O$
7H-5, 91	61.61	1.2512	−0.490	2.681
7H-5, 120	61.90	1.2558	−0.534	2.517
7H-5, 120	61.90	1.2558	−0.398	2.721
7H-6, 11	62.31	1.2623	−0.975	2.469
7H-6, 11	62.31	1.2623	−0.562	2.822
7H-6, 30	62.50	1.2653	−1.506	2.417
7H-6, 30	62.50	1.2653	−1.549	2.418
7H-6, 60	62.80	1.2701	−1.409	2.433
7H-6, 60	62.80	1.2701	−1.607	2.408
7H-6, 90	63.10	1.2748	−1.055	2.431
8H-1, 30	64.50	1.2970	1.145	2.889
8H-1, 81	65.01	1.3051	0.118	2.374
8H-1, 111	65.31	1.3099	0.496	2.490
8H-1, 140	65.60	1.3145	−0.214	2.526
8H-1, 140	65.60	1.3145	−0.299	2.440
8H-2, 30	66.00	1.3208	−0.592	2.444
8H-2, 51	66.21	1.3241	−0.608	2.324
8H-2, 81	66.51	1.3289	−0.682	2.149
8H-2, 81	66.51	1.3289	−0.665	1.998
8H-2, 111	66.81	1.3336	−0.998	1.907
8H-2, 140	67.10	1.3382	0.023	2.226
8H-3, 31	67.51	1.3447	0.958	2.487
8H-3, 48	67.68	1.3474	0.420	2.337
8H-3, 82	68.02	1.3528	−0.148	2.505
8H-3, 82	68.02	1.3528	−0.141	2.910
8H-3, 111	68.31	1.3574	−0.319	2.675
8H-3, 140	68.60	1.3620	0.094	2.702
8H-4, 31	69.01	1.3685	−0.339	2.162
8H-4, 31	69.01	1.3685	−0.332	2.139
8H-4, 51	69.21	1.3717	−0.012	2.223
8H-4, 81	69.51	1.3764	−0.793	2.318
8H-4, 81	69.51	1.3764	−0.647	2.544
8H-4, 111	69.81	1.3812	−0.563	2.675
8H-4, 140	70.10	1.3858	0.066	2.708
8H-5, 31	70.51	1.3923	−0.439	2.780
8H-5, 51	70.71	1.3955	−0.388	2.602
8H-5, 81	71.01	1.4002	−0.379	2.512
8H-5, 81	71.01	1.4002	−0.709	2.432
8H-5, 111	71.31	1.4050	−0.606	2.419
8H-5, 140	71.60	1.4096	−0.826	2.081
8H-6, 31	72.01	1.4161	−0.525	2,437
8H-6, 51	72.21	1.4192	−0.413	2.301
8H-6, 81	72.51	1.4240	−0.326	2.031
8H-6, 111	72.81	1.4287	−0.552	2.183
9H-1, 51	74.21	1.4509	−0.064	2.237
9H-1, 51	74.21	1.4509	−0.012	2.436
9H-1, 81	74.51	1.4557	0.069	2.093
9H-1, 111	74.81	1.4604	0.313	2.448
9H-1, 141	75.11	1.4652	0.155	2.087
9H-2, 21	75.41	1.4700	0.242	2.257
9H-2, 51	75.71	1.4747	0.046	2.396
9H-2, 81	76.01	1.4795	−0.092	2.606
9H-2, 111	76.31	1.4842	0.001	2.491
9H-2, 141	76.61	1.4890	0.013	2.438
9H-3, 21	76.91	1.4937	0.012	2.472
9H-3, 51	77.21	1.4985	0.197	2.600
9H-3, 81	77.51	1.5032	0.046	2.489
9H-3, 111	77.81	1.5080	0.050	2.378
9H-3, 141	78.11	1.5128	0.178	2.615
9H-4, 21	78.41	1.5175	0.415	2.688
9H-4, 51	78.71	1.5223	0.493	2.615
9H-4, 81	79.01	1.5270	0.445	2.397
9H-4, 81	79.01	1.5270	0.376	2.373
9H-5, 21	79.91	1.5413	−0.296	2.732
9H-7, 21	82.91	1.5888	−0.693	2.640
9H-7, 21	82.91	1.5888	−0.981	2.519
10H-1, 20	83.40	1.5966	−0.183	2.652
10H-1, 20	83.40	1.5966	−0.264	2.077
10H-1, 20	83.40	1.5966	−0.492	2.182
10H-1, 20	83.40	1.5966	−0.186	2.527
10H-2, 20	84.90	1.6204	−1.184	2.302
10H-3, 20	86.40	1.6442	−1.504	2.026
10H-4, 20	87.90	1.6690	−0.794	2.552
10H-4, 20	87.90	1.6690	−0.686	2.536
10H-5, 20	89.40	1.6958	0.309	2.400
10H-5, 20	89.40	1.6958	0.290	2.362
10H-6, 20	90.90	1.7227	−0.172	2.165

Table 3 (continued).

Core, section, interval (cm)	Depth (mbsf)	Age (Ma)	$\delta^{13}C$	$\delta^{18}O$
10H-7, 20	92.40	1.7495	−0.581	2.491
11H-1, 21	92.91	1.7586	−0.431	2.208
11H-1, 21	92.91	1.7586	−0.157	2.107
11H-2, 21	94.41	1.7855	−0.108	2.265
11H-3, 21	95.91	1.8123	−0.556	2.446
11H-3, 21	95.91	1.8123	−1.341	2.144
11H-3, 21	95.91	1.8123	−0.784	2.357
11H-3, 21	95.91	1.8123	−1.516	2.165
11H-3, 21	95.91	1.8123	−0.740	2.339
11H-4, 21	97.41	1.8392	−0.894	2.524
11H-4, 21	97.41	1.8392	−0.885	2.447
11H-5, 21	98.91	1.8660	−0.440	2.260
11H-5, 21	98.91	1.8660	−0.430	2.238
11H-5, 21	98.91	1.8660	−0.605	2.366
11H-6, 21	100.41	1.8913	−0.155	2.273
11H-6, 21	100.41	1.8913	−0.181	2.284
12H-1, 21	102.41	1.9073	−0.315	2.331
12H-1, 21	102.41	1.9073	−0.250	2.298
12H-1, 21	102.41	1.9073	−0.263	2.318
12H-2, 21	103.91	1.9193	0.210	2.725
12H-2, 21	103.91	1.9193	0.197	2.715
12H-3, 21	105.41	1.9313	−0.220	2.331
12H-3, 21	105.41	1.9313	−0.206	2.309
12H-3, 21	105.41	1.9313	−0.332	2.253
12H-4, 21	106.91	1.9433	−0.357	2.787
12H-4, 21	106.91	1.9433	−0.348	2.720
12H-4, 21	106.91	1.9433	−0.527	2.320
12H-5, 21	108.41	1.9553	0.392	2.189
12H-5, 21	108.41	1.9553	0.434	2.420
12H-5, 21	108.41	1.9553	0.381	2.515
12H-6, 21	109.91	1.9673	−0.064	2.899
13H-1, 21	111.91	1.9833	−0.420	2.476
13H-2, 21	113.41	1.9953	−0.390	2.271
13H-3, 21	114.91	2.0073	−0.429	2.795
13H-4, 21	116.41	2.0193	−0.330	2.422
13H-5, 21	117.91	2.0313	−0.205	2.730
13H-6, 21	119.41	2.0433	−0.077	2.662
13H-7, 21	120.91	2.0553	0.148	2.239
13H-7, 21	120.91	2.0553	0.415	2.514
14H-1, 21	121.41	2.0593	−0.240	2.509
14H-2, 21	122.91	2.0713	−0.423	2.517
14H-3, 21	124.41	2.0833	−0.504	2.292
14H-4, 21	125.91	2.0953	0.312	2.754
14H-5, 21	127.41	2.1073	0.015	2.762
14H-6, 21	128.91	2.1193	−0.341	2.427
15H-1, 21	130.91	2.1353	−0.205	1.897
15H-1, 21	130.91	2.1353	−0.152	2.001
15H-1, 21	130.91	2.1353	−0.726	1.605
15H-2, 21	132.41	2.1481	−0.227	2.217
15H-2, 21	132.41	2.1481	−0.340	2.227
15H-3, 21	133.91	2.1614	−0.114	2.126
15H-3, 141	135.11	2.1720	−0.197	2.085
15H-5, 21	137.21	2.1906	−0.580	2.461
15H-6, 21	138.41	2.2013	−0.014	2.158
15H-7, 21	139.91	2.2146	−0.627	2.026
16H-1, 21	140.41	2.2190	−0.943	1.730
16H-2, 21	141.91	2.2323	−0.636	2.223
16H-3, 21	143.41	2.2456	−0.723	2.023
16H-4, 21	144.91	2.2589	−0.114	2.823
16H-5, 21	146.41	2.2722	0.006	2.336
16H-6, 21	147.91	2.2855	−0.423	2.269
17X-1, 21	149.91	2.3032	−0.477	1.952
17X-2, 21	151.41	2.3165	−0.068	2.829
17X-3, 21	152.91	2.3298	−0.250	2.509
17X-3, 21	152.91	2.3298	−0.276	2.318
17X-4, 21	154.41	2.3431	−0.847	2.039
17X-5, 21	155.91	2.3564	−0.537	2.620
17X-6, 21	157.41	2.3697	−0.594	2.364
18X-1, 21	159.41	2.3875	−0.044	2.345
18X-2, 21	160.91	2.4008	0.081	2.337
18X-3, 21	162.41	2.4141	−0.017	2.587
18X-4, 21	163.91	2.4274	−0.157	2.739
18X-5, 21	165.41	2.4407	0.025	2.108
18X-6, 21	166.91	2.4540	−0.420	2.532
19X-1, 21	168.91	2.5488	−0.092	2.893
19X-2, 21	170.41	2.6873	0.830	2.589
19X-3, 21	171.91	2.7428	0.955	2.758

Table 3 (continued).

Core, section, interval (cm)	Depth (mbsf)	Age (Ma)	$\delta^{13}C$	$\delta^{18}O$
19X-4, 21	173.41	2.7983	0.466	2.454
19X-4, 21	173.41	2.7983	0.428	2.529
19X-5, 21	174.91	2.8538	1.783	3.470
19X-6, 21	176.41	2.9093	1.783	3.372
20X-1, 21	178.41	3.0295	1.221	2.998
20X-2, 21	179.91	3.1238	0.508	2.358
20X-2, 21	179.91	3.1238	0.544	2.439
20X-3, 21	181.41	3.1911	2.247	3.576
20X-3, 21	181.41	3.1911	2.177	3.343
20X-4, 21	182.91	3.2504	1.493	2.966
20X-5, 21	184.41	3.3098	2.002	2.745
20X-6, 21	185.91	3.3691	0.515	2.156
20X-6, 21	185.91	3.3691	0.598	2.104
20X-6, 21	185.91	3.3691	0.661	1.734
20X-7, 21	187.41	3.4380	0.190	2.044
20X-7, 21	187.41	3.4380	1.095	2.875
21X-1, 46	188.16	3.4775	0.422	2.112
21X-1, 51	188.21	3.4802	0.228	2.038
21X-2, 46	189.66	3.5567	0.436	2.059
21X-2, 46	189.66	3.5567	0.438	2.090
21X-3, 46	191.16	3.6358	0.424	1.911
22X-1, 21	197.41	3.9037	0.599	2.081
22X-2, 21	198.91	3.9257	0.759	2.243
22X-2, 21	198.91	3.9257	0.730	2.227
22X-3, 21	200.41	3.9476	1.576	2.222
22X-3, 51	200.71	3.9520	1.661	2.651
22X-4, 21	201.91	3.9696	1.663	2.688
22X-4, 51	202.21	3.9856	1.084	2.617
22X-5, 21	203.41	4.0549	2.576	2.740
22X-5, 51	203.71	4.0723	2.590	3.198
22X-5, 140	204.60	4.1094	1.656	2.482
23X-1, 21	206.91	4.1624	0.550	2.118
23X-1, 51	207.21	4.1693	0.464	2.026
23X-2, 21	208.41	4.1969	0.463	2.128
23X-3, 21	209.91	4.2313	0.370	2.072
23X-3, 51	210.21	4.2382	0.326	1.841
23X-4, 21	211.41	4.3454	0.816	2.278
23X-4, 51	211.71	4.3737	1.049	2.332
23X-5, 21	212.91	4.4524	0.672	2.286
23X-6, 21	214.41	4.4992	1.448	2.485
24X-1, 21	216.41	4.5484	0.990	2.241
24X-2, 21	217.91	4.6277	0.659	2.113
24X-3, 21	219.41	4.7672	0.808	1.996
24X-3, 51	219.71	4.7893	0.963	2.062
24X-4, 51	221.21	4.8967	2.010	2.904
24X-5, 21	222.41	4.9825	0.583	2.417
24X-5, 51	222.71	5.0040	1.276	2.388
24X-6, 21	223.91	5.0899	1.065	2.318
25X-1, 21	225.91	5.3801	1.658	2.302
25X-2, 21	227.41	5.4242	1.234	2.048
25X-2, 48	227.68	5.4322	1.149	1.991
25X-3, 21	228.91	5.4684	1.711	2.335
25X-4, 21	230.41	5.5126	1.928	2.822
25X-6, 21	233.41	5.6505	1.769	2.605
114-704B-				
1H-1, 31	0.31	0.0530	0.031	2.365
1H-1, 61	0.61	0.1043	−0.002	2.338
1H-1, 90	0.90	0.1540	0.254	2.378
1H-1, 121	1.21	0.1971	0.721	2.598
1H-2, 31	1.81	0.2148	0.493	1.861
1H-2, 61	2.11	0.2236	−0.082	1.514
1H-2, 90	2.40	0.2322	0.151	1.361
1H-2, 121	2.71	0.2413	0.186	1.593
1H-3, 45	3.45	0.2631	−0.629	1.740
1H-3, 102	4.02	0.2799	0.225	2.110
1H-4, 142	5.92	0.3360	2.988	3.799
1H-5, 20	6.20	0.3442	3.088	3.005
1H-5, 45	6.45	0.3516	2.637	3.062
2H-1, 8	6.78	0.3613	2.695	3.199
2H-1, 43	7.13	0.3717	1.504	2.835
2H-1, 108	7.78	0.3908	2.999	3.415
2H-1, 143	8.13	0.4012	1.497	3.237
2H-2, 61	8.81	0.4212	1.780	3.052
2H-2, 122	9.42	0.4392	1.345	2.704
2H-3, 18	9.88	0.4528	1.343	2.680
2H-3, 62	10.32	0.4658	0.106	2.730

Table 3 (continued).

Core, section, interval (cm)	Depth (mbsf)	Age (Ma)	$\delta^{13}C$	$\delta^{18}O$
2H-3, 103	10.73	0.4778	−0.132	2.459
2H-3, 140	11.10	0.4888	−0.089	2.214
2H-4, 17	11.37	0.4967	0.144	2.358
2H-4, 58	11.78	0.5088	−0.332	1.301
2H-4, 99	12.19	0.5209	−0.200	2.252
2H-4, 99	12.19	0.5209	−0.599	1.893
2H-4, 99	12.19	0.5209	−0.600	1.971
2H-4, 138	12.58	0.5324	−1.029	2.534
2H-5, 15	12.85	0.5404	−0.844	2.386
2H-5, 55	13.25	0.5522	−1.154	2.429
2H-5, 97	13.67	0.5646	−1.156	2.719
2H-5, 137	14.07	0.5764	−0.894	2.268
3H-1, 21	16.41	0.6250	−1.367	2.486
3H-1, 61	16.81	0.6273	−0.886	2.644
3H-1, 95	17.15	0.6293	−0.598	2.765
3H-1, 141	17.61	0.6320	−0.765	2.893
3H-2, 21	17.91	0.6337	−2.165	2.209
3H-2, 21	17.91	0.6337	−2.299	1.553
3H-2, 61	18.31	0.6360	−0.664	1.998
3H-2, 95	18.65	0.6380	0.370	2.368
3H-2, 141	19.11	0.6407	0.248	2.272
3H-3, 21	19.41	0.6424	0.336	2.304
3H-3, 21	19.41	0.6424	−0.361	2.551
3H-3, 61	19.81	0.6447	1.446	2.593
3H-3, 95	20.15	0.6467	1.648	2.473
3H-3, 141	20.61	0.6494	−0.542	2.680
3H-4, 21	20.91	0.6511	−0.268	2.809
3H-4, 61	21.31	0.6534	−0.351	2.821
3H-4, 95	21.65	0.6554	−0.447	2.798
3H-4, 141	22.11	0.6581	−0.397	2.755
3H-5, 21	22.41	0.6598	0.586	2.398
3H-5, 61	22.81	0.6621	−1.122	1.965
3H-5, 95	23.15	0.6641	−1.511	2.373
3H-5, 141	23.61	0.6668	−0.307	2.865
3H-6, 21	23.91	0.6685	−0.845	1.944
3H-6, 21	23.91	0.6685	−1.233	1.673
3H-6, 61	24.31	0.6708	−1.634	2.280
3H-6, 95	24.65	0.6728	−0.252	2.088
3H-6, 141	25.11	0.6755	−0.458	2.330
3H-7, 21	25.41	0.6772	−0.840	2.500
3H-7, 61	25.81	0.6795	−0.185	2.616
4H-1, 31	26.01	0.6807	−1.108	2.046
4H-1, 71	26.41	0.6830	−1.654	2.149
4H-1, 106	26.76	0.6850	−0.718	2.121
4H-1, 121	26.91	0.6859	−1.308	2.731
4H-1, 146	27.16	0.6874	−0.532	2.969
4H-2, 31	27.51	0.6894	0.045	2.609
4H-2, 71	27.91	0.6917	−0.493	2.446
4H-2, 106	28.26	0.6937	−0.802	2.687
4H-2, 121	28.41	0.6946	−0.710	2.430
4H-2, 146	28.66	0.6961	−0.921	2.906
4H-2, 146	28.66	0.6961	−2.289	1.182
4H-3, 31	29.01	0.6981	0.360	2.486
4H-3, 71	29.41	0.7004	0.376	2.186
4H-3, 106	29.76	0.7024	−1.511	1.659
4H-3, 121	29.91	0.7033	−0.701	1.960
4H-3, 146	30.16	0.7048	−1.165	1.978
4H-4, 31	30.51	0.7068	−0.658	2.201
4H-4, 71	30.91	0.7091	−0.624	2.157
4H-4, 106	31.26	0.7111	−0.781	2.081
4H-4, 146	31.60	0.7131	−0.337	2.326
4H-5, 31	32.01	0.7155	−0.781	2.710
4H-5, 40	32.10	0.7160	0.711	2.793
4H-5, 71	32.41	0.7178	−0.983	2.399
4H-5, 106	32.76	0.7199	−1.108	2.421
4H-5, 121	32.91	0.7207	−0.870	3.947
4H-5, 146	33.16	0.7222	−0.644	2.591
4H-6, 31	33.51	0.7242	−0.486	2.432
4H-6, 71	33.91	0.7265	−0.186	2.328
4H-6, 106	34.26	0.7286	1.340	3.085
24X-1, 21	213.91	4.4870	0.700	2.449
24X-1, 51	214.21	4.4943	0.786	1.736
24X-1, 81	214.51	4.5017	1.288	2.434
24X-1, 111	214.81	4.5091	0.628	2.281
24X-1, 141	215.11	4.5164	0.918	2.057
24X-2, 21	215.41	4.5238	0.470	2.007
24X-2, 51	215.71	4.5312	0.505	1.975

Table 3 (continued).

Core, section, interval (cm)	Depth (mbsf)	Age (Ma)	$\delta^{13}C$	$\delta^{18}O$
24X-2, 81	216.01	4.5386	0.468	1.612
24X-2, 115	216.35	4.5469	0.647	2.460
24X-2, 141	216.61	4.5533	0.883	2.445
24X-3, 21	216.91	4.5607	0.644	2.201
24X-3, 51	217.21	4.5680	0.999	1.770
24X-3, 81	217.51	4.5905	0.992	2.109
24X-3, 111	217.81	4.6184	0.224	1.861
24X-3, 141	218.11	4.6463	0.392	1.648
24X-4, 21	218.41	4.6742	0.510	1.854
24X-4, 51	218.71	4.7021	0.947	1.768
24X-4, 81	219.01	4.7300	0.842	2.071
24X-4, 111	219.31	4.7579	0.510	1.800
24X-4, 111	219.31	4.7579	0.832	1.855
24X-4, 141	219.61	4.7822	0.775	1.754
24X-5, 21	219.91	4.8036	0.652	1.970
24X-5, 51	220.21	4.8251	0.717	1.924
24X-5, 111	220.81	4.8680	0.779	1.870
24X-5, 141	221.11	4.8895	1.252	1.669
24X-6, 10	221.30	4.9031	1.453	2.317
24X-6, 41	221.61	4.9253	1.048	1.985
24X-6, 71	221.91	4.9468	0.879	1.471
24X-6, 111	222.31	4.9754	0.546	1.707
24X-6, 141	222.61	4.9969	0.943	1.946
24X-7, 41	223.11	5.0326	1.010	1.662
24X-7, 51	223.21	5.0398	1.216	1.932
25X-1, 21	223.41	5.0541	1.734	2.269
25X-1, 51	223.71	5.0756	1.464	2.463
25X-1, 109	224.29	5.1171	1.088	2.053
25X-1, 141	224.61	5.1400	1.177	2.013
25X-2, 21	224.91	5.3506	1.288	1.884
25X-2, 51	225.21	5.3594	1.012	1.397
25X-2, 81	225.51	5.3683	1.871	2.104
25X-2, 109	225.79	5.3765	1.334	2.120
25X-2, 141	226.11	5.3859	0.278	1.629
25X-2, 141	226.11	5.3859	0.331	1.846
25X-2, 141	227.61	5.4301	1.139	2.086
25X-3, 21	226.41	5.3948	0.335	1.864
25X-3, 21	226.41	5.3948	0.412	2.046
25X-3, 51	226.71	5.4036	1.144	1.980
25X-3, 81	227.01	5.4125	1.268	2.016
25X-3, 109	227.29	5.4207	1.095	2.012
25X-4, 21	227.91	5.4390	0.750	2.144
25X-4, 51	228.21	5.4478	1.254	0.871
25X-4, 51	228.21	5.4478	1.312	0.770
25X-4, 81	228.51	5.4567	1.288	2.504
25X-4, 109	228.79	5.4649	1.845	2.463
25X-4, 141	229.11	5.4743	1.584	2.172
25X-5, 21	229.41	5.4832	1.314	2.202
25X-5, 51	229.71	5.4920	2.034	2.148
25X-5, 81	230.01	5.5008	1.758	2.634
25X-5, 109	230.29	5.5091	1.026	2.404
25X-5, 141	230.61	5.5185	1.243	1.344
25X-6, 21	230.91	5.5274	1.947	2.906
25X-6, 51	231.21	5.5405	1.462	1.878
25X-6, 81	231.51	5.5555	2.109	2.627
25X-6, 109	231.79	5.5695	1.748	2.775
25X-6, 141	232.11	5.5855	1.634	2.043
25X-7, 21	232.41	5.6005	1.200	2.438
25X-7, 51	232.71	5.6155	1.828	1.964
26X-1, 51	233.21	5.6405	1.749	1.952
26X-1, 111	233.81	5.6705	1.386	2.410
26X-1, 141	234.11	5.6831	1.285	2.101
26X-2, 21	234.41	5.6915	1.488	2.447
26X-2, 51	234.71	5.6999	1.253	2.354
26X-2, 81	235.01	5.7083	1.351	2.330
26X-2, 111	235.31	5.7167	1.603	2.411
26X-2, 141	235.61	5.7251	1.678	2.172
26X-3, 21	235.91	5.7335	1.105	2.179
26X-3, 51	236.21	5.7419	1.112	1.636
26X-3, 111	236.81	5.7587	1.138	2.160
26X-3, 141	237.11	5.7671	1.264	2.221
26X-4, 21	237.41	5.7755	0.970	2.191
26X-4, 81	238.01	5.7923	1.271	2.149
26X-4, 81	238.01	5.7923	1.372	2.596
26X-4, 111	238.31	5.8007	1.294	2.604
26X-5, 21	238.91	5.8175	2.072	2.980
26X-5, 51	239.21	5.8259	2.617	3.026

Table 3 (continued).

Core, section, interval (cm)	Depth (mbsf)	Age (Ma)	$\delta^{13}C$	$\delta^{18}O$
26X-5, 51	239.21	5.8259	2.597	3.084
26X-5, 51	239.21	5.8259	2.703	3.417
26X-6, 21	240.41	5.8595	2.422	3.365
27X-1, 141	243.61	5.9847	1.516	1.995
27X-1, 141	243.61	5.9847	1.557	1.995
27X-2, 51	244.21	6.0116	1.205	2.371
27X-2, 111	244.81	6.0385	1.380	2.023
27X-2, 141	245.11	6.0519	1.302	2.448
27X-2, 141	245.11	6.0519	1.406	2.695
27X-3, 21	245.41	6.0654	1.425	2.744
27X-3, 51	245.71	6.0789	1.492	2.099
27X-3, 51	245.71	6.0789	1.618	2.425
27X-3, 111	246.31	6.1058	1.515	2.471
27X-3, 141	246.61	6.1192	1.420	2.074
27X-3, 141	246.61	6.1192	1.445	2.038
27X-4, 15	246.85	6.1300	1.476	2.434
27X-4, 51	247.21	6.1462	1.616	2.325
27X-4, 111	247.81	6.1731	1.640	2.422
27X-4, 141	248.11	6.1865	2.512	2.608
27X-4, 141	248.11	6.1865	2.448	2.571
27X-4, 141	248.11	6.1865	2.409	2.380
27X-4, 141	248.11	6.1865	2.555	2.548
27X-5, 21	248.41	6.2000	1.766	2.628
27X-5, 51	248.71	6.2134	1.800	2.971
27X-5, 111	249.31	6.2404	1.444	2.058
27X-6, 21	249.91	6.2673	1.074	2.494
27X-6, 51	250.21	6.2807	1.581	2.556
27X-6, 51	250.21	6.2807	1.593	2.779
27X-6, 111	250.81	6.3076	1.581	2.495
27X-6, 141	251.11	6.3211	1.747	2.230
27X-6, 141	251.11	6.3211	1.670	2.359
27X-7, 21	251.41	6.3346	1.850	2.503
27X-7, 51	251.71	6.3480	1.884	2.272
27X-7, 51	251.71	6.3480	1.826	2.437
28X-1, 21	251.91	6.3570	2.286	3.087
28X-1, 50	252.20	6.3700	2.271	2.877
28X-1, 50	252.20	6.3700	2.288	2.762
28X-1, 100	252.70	6.3823	2.656	3.235
28X-1, 141	253.11	6.3923	2.581	3.191
28X-2, 21	253.41	6.3997	2.521	3.124
28X-2, 50	253.70	6.4068	2.409	2.871
28X-2, 80	254.00	6.4142	2.263	2.815
28X-2, 80	254.00	6.4142	2.366	2.887
28X-2, 100	254.20	6.4191	2.265	3.095
28X-2, 141	254.61	6.4291	1.857	2.672
28X-3, 21	254.91	6.4365	1.364	2.298
28X-3, 50	255.20	6.4436	2.221	3.001
28X-3, 100	255.70	6.4559	2.552	3.249
28X-3, 141	256.11	6.4659	2.092	2.656
28X-4, 21	256.41	6.4733	2.088	2.938
28X-4, 50	256.70	6.4804	2.208	2.613
28X-4, 50	256.70	6.4804	2.307	2.743
28X-4, 80	257.00	6.4877	2.390	3.141
28X-4, 111	257.31	6.4953	2.128	2.726
28X-4, 141	257.61	6.5110	1.781	2.746
28X-5, 21	257.91	6.5410	1.643	2.477
28X-5, 50	258.20	6.5700	2.223	2.978
28X-5, 50	258.20	6.5700	2.163	3.088
28X-5, 111	258.81	6.6310	2.030	2.689
28X-5, 141	259.11	6.6610	2.268	2.844
28X-6, 21	259.41	6.6910	2.004	2.792
28X-6, 50	259.70	6.7032	2.253	2.478
28X-6, 80	260.00	6.7080	1.822	2.529
28X-6, 100	260.20	6.7112	2.230	2.898
28X-6, 141	260.61	6.7178	2.067	2.702
28X-6, 141	260.61	6.7178	2.049	2.381
28X-7, 21	260.91	6.7226	2.246	2.867
28X-7, 50	261.20	6.7272	2.329	2.695
29X-1, 21	261.41	6.7306	2.040	2.801
29X-1, 51	261.71	6.7354	1.767	2.535
29X-1, 111	262.31	6.7450	1.653	2.378
29X-1, 141	262.61	6.7498	2.292	2.914
29X-2, 21	262.91	6.7546	2.303	2.964
29X-2, 51	263.21	6.7594	2.618	3.037
29X-2, 51	263.21	6.7594	2.555	2.844
29X-2, 81	263.51	6.7642	2.622	3.008
29X-2, 81	263.51	6.7642	2.690	3.215

Table 3 (continued).

Core, section, interval (cm)	Depth (mbsf)	Age (Ma)	$\delta^{13}C$	$\delta^{18}O$
29X-2, 111	263.81	6.7690	2.406	3.105
29X-2, 141	264.11	6.7738	2.167	2.755
29X-3, 21	264.41	6.7786	2.243	2.869
29X-3, 51	264.71	6.7947	2.251	2.834
29X-3, 111	265.31	6.8367	2.214	2.792
29X-3, 141	265.61	6.8737	2.219	2.955
29X-4, 21	265.91	6.9382	2.427	2.926
29X-4, 51	266.21	7.0027	2.068	2.568
29X-4, 81	266.51	7.0672	1.826	2.685
29X-4, 81	266.51	7.0672	1.762	2.353
29X-4, 81	266.51	7.0672	1.802	2.370
29X-4, 110	266.80	7.1295	1.574	2.497
29X-4, 141	267.11	7.1962	1.781	2.427
29X-5, 21	267.41	7.2607	1.607	2.654
29X-5, 51	267.71	7.2854	2.180	2.668
29X-5, 111	268.31	7.3010	2.037	2.633
29X-6, 21	268.91	7.3166	1.954	2.752
29X-6, 51	269.21	7.3243	1.886	1.685
29X-6, 81	269.51	7.3321	1.683	2.420
29X-6, 81	269.51	7.3321	1.676	2.287
29X-6, 81	269.51	7.3321	1.553	1.983
29X-6, 110	269.80	7.3396	2.006	2.473
29X-7, 21	270.41	7.3525	1.831	2.630
29X-7, 51	270.71	7.3561	2.308	2.369
29X-7, 51	270.71	7.3561	2.288	2.498
29X-7, 51	270.71	7.3561	2.120	2.220
29X-7, 51	270.71	7.3561	2.196	2.069
30X-1, 21	270.91	7.3584	2.630	3.345
30X-1, 51	271.21	7.3621	2.563	2.999
30X-1, 51	271.21	7.3621	2.634	3.193
30X-1, 111	271.81	7.3693	1.897	2.722
30X-1, 141	272.11	7.3729	2.033	2.591
30X-2, 21	272.41	7.3765	1.947	2.841
30X-2, 37	272.57	7.3784	1.585	2.221
30X-2, 37	272.57	7.3784	1.583	2.210
30X-2, 51	272.71	7.3801	2.078	2.684
30X-2, 81	273.01	7.3837	1.444	2.190
30X-2, 111	273.31	7.3873	1.395	2.442
30X-3, 21	273.91	7.3945	2.304	2.883
30X-3, 51	274.21	7.3981	2.450	2.728
30X-3, 111	274.81	7.4053	2.518	3.160
30X-3, 141	275.11	7.4089	2.311	2.564
30X-4, 21	275.41	7.4170	2.271	2.864
30X-4, 51	275.71	7.4269	2.233	2.606
30X-4, 81	276.01	7.4368	2.251	2.659
30X-4, 111	276.31	7.4468	2.108	2.693
30X-4, 141	276.61	7.4567	2.347	2.942
30X-5, 21	276.91	7.4666	2.424	2.948
30X-5, 51	277.21	7.4766	2.094	2.377
30X-6, 21	278.41	7.5163	1.887	2.749
30X-7, 20	279.90	7.5656	1.683	2.630
30X-7, 51	280.21	7.5759	1.528	2.274
30X-7, 51	280.21	7.5759	1.570	2.296
31X-1, 21	280.41	7.5825	1.960	2.448
31X-1, 51	280.71	7.5924	1.957	2.377
31X-1, 111	281.31	7.6123	1.768	2.685
31X-1, 141	281.61	7.6222	1.518	2.189
31X-2, 20	281.90	7.6318	1.355	2.046
31X-2, 51	282.21	7.6421	1.472	1.993
31X-2, 81	282.51	7.6520	1.915	2.543
31X-2, 111	282.81	7.6620	1.872	2.779
31X-2, 141	283.11	7.6719	2.169	2.705
31X-3, 20	283.40	7.6815	2.198	2.986
31X-3, 51	283.71	7.6918	2.476	2.909
31X-3, 111	284.31	7.7116	2.530	3.241
31X-3, 141	284.61	7.7216	2.275	2.611
31X-4, 20	284.90	7.7312	2.234	2.672
31X-4, 81	285.51	7.7513	2.191	2.441
31X-4, 141	286.11	7.7712	1.745	2.055
31X-5, 20	286.40	7.7808	1.788	2.457
31X-5, 51	286.71	7.7911	1.759	2.421
31X-5, 111	287.31	7.8106	1.936	2.336
31X-5, 141	287.61	7.8209	2.243	2.498
31X-6, 20	287.90	7.8305	1.539	2.189
31X-6, 51	288.21	7.8407	2.007	2.272
31X-6, 81	288.51	7.8507	1.362	2.008
31X-6, 110	288.80	7.8603	1.386	2.050
31X-6, 141	289.11	7.8705	1.970	2.057
31X-7, 46	289.66	7.8887	2.348	2.886

3.5°/oo. At this point, $\delta^{18}O$ decreases rapidly to 2.5°/oo by 170 mbsf (2.67 Ma), where it oscillates about the mean with variability of 0.3°/oo to 5°/oo to the present day. Variability increases above about 40 mbsf. A temporary maximum occurs at 11 to 5 mbsf (0.49–0.31 Ma), followed by a local minimum at about 2.5 mbsf (0.24 Ma).

Carbon Isotopes

The record of fine-fraction $\delta^{13}C$ shows a different character than that of $\delta^{18}O$ (Fig. 2 and Table 3). Between 290 and about 255 mbsf (7.9–6.44 Ma), $\delta^{13}C$ is roughly constant, averaging about 2°/oo. At this point, fine-fraction $\delta^{13}C$ begins to decrease, reaching a minimum of 0.33°/oo at 210.2 mbsf (4.23 Ma). This decrease in $\delta^{13}C$, roughly coincident with the late Miocene carbon shift (Keigwin and Shackleton, 1980), is observed in the planktonic and benthic foraminiferal records, but the shift in the fine fraction occurs across a period of about 2 m.y. rather than a few hundred thousand years as found in the foraminiferal records. The sampling frequency is somewhat less from this point upward, but it appears that $\delta^{13}C$ becomes more variable, with spikes of high $\delta^{13}C$ values occurring at about 203.5 mbsf (4.06 Ma), 181 mbsf (3.17 Ma), 175 mbsf (2.86 Ma), and 171 mbsf (2.71 Ma).

Between 170.41 and 168.91 mbsf (2.69–2.55 Ma), a sudden shift in $\delta^{13}C$ occurs, with $\delta^{13}C$ falling from an average of 1.26°/oo between the base of the Gauss and the shift to an average of −0.22°/oo between the shift and the top of the Matuyama, for a total change of −1.48°/oo.

The amplitude of variability above the Gauss/Matuyama boundary is small up to about 75 mbsf (1.46 Ma). Above 75 mbsf, large swings in $\delta^{13}C$ occur, with both the highest and lowest $\delta^{13}C$ values measured at Site 704 found in this interval. Maxima occur at 61.00 mbsf (1.24 Ma), 36.51 mbsf (0.78 Ma), and 5.75 mbsf (0.33 Ma). The increase to the 36.51 mbsf maximum is fairly smooth, beginning with a minimum of 1.84°/oo at 52.90 mbsf (1.11 Ma) and ending at 3.23°/oo. A similar trend occurs in the buildup to a 6 mbsf maximum, starting with a minimum of −2.30°/oo at 17.91 mbsf (0.63 Ma) and increasing to 3.14°/oo.

The meaning of the younger events is unclear, because of the disturbed nature of the upper 50 m (Shipboard Scientific Party, 1988). This disturbance can affect our knowledge of the timing and magnitude of the events. However, core disturbance would be expected to homogenize and decrease the magnitude of the signals seen. The magnitude of these changes (up to 5.52°/oo for $\delta^{13}C$ between 36.51 and 28.66 mbsf and 2.77°/oo for $\delta^{18}O$ between 32.91 and 28.66 mbsf) must therefore be minimum magnitudes. Clearly, extremely large changes in fine-fraction isotopic composition in the upper 75 m of Site 704 have occurred.

Changes in the Fine-Fraction Composition

Results of random-settling slide analysis show that changes have indeed occurred in the particle composition of the fine fraction (Fig. 4 and Table 4). Significant changes occurred at 170–160, 150–140, 110–100, and 90–80 mbsf and every 10 m above the latter depth to a depth of 60 mbsf, the shallowest sample thus far examined. From 170 to 160 mbsf, the nannofossil content of the fine fraction drops from over 90% to about 40%, whereas micrite content rises from near 0% to approximately 60%. From 150 to 140 mbsf, nannofossil content rises again to about 90%, whereas micrite content falls to about 10%. Nannofossil content again drops to about 50% between 110 and 100 mbsf with micrite rising proportionately. Nannofossil and micrite contents fluctuate widely every 10 m above this point, with foraminiferal content becoming important only at 60 mbsf. There is a general increase upward of the micrite content, contrary to the

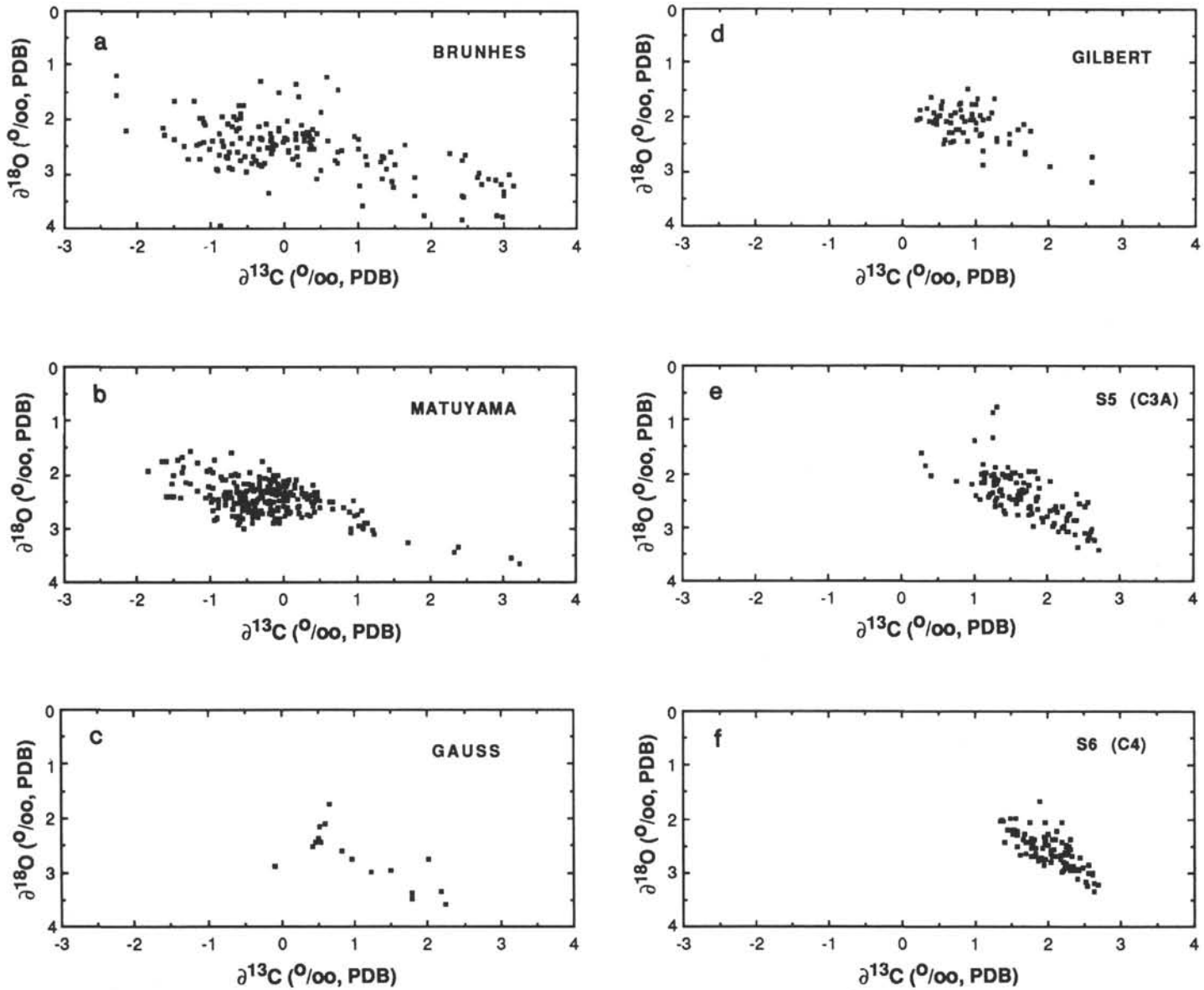

Figure 3. Covariance between fine-fraction $\delta^{13}C$ and $\delta^{18}O$ for different paleomagnetic polarity intervals: Brunhes (0–34.51 mbsf, 0–0.73 Ma), Matuyama (34.51–168.72 mbsf, 0.73–2.47 Ma), Gauss (168.72–189.69 mbsf, 2.47–3.40 Ma), Gilbert (189.69–224.89 mbsf, 3.40–5.35 Ma), S5 (C3A) (224.89–259.50 mbsf, 5.35–6.70 Ma), and S6 (C4) (259.50–290.00 mbsf, 6.70–7.90 Ma).

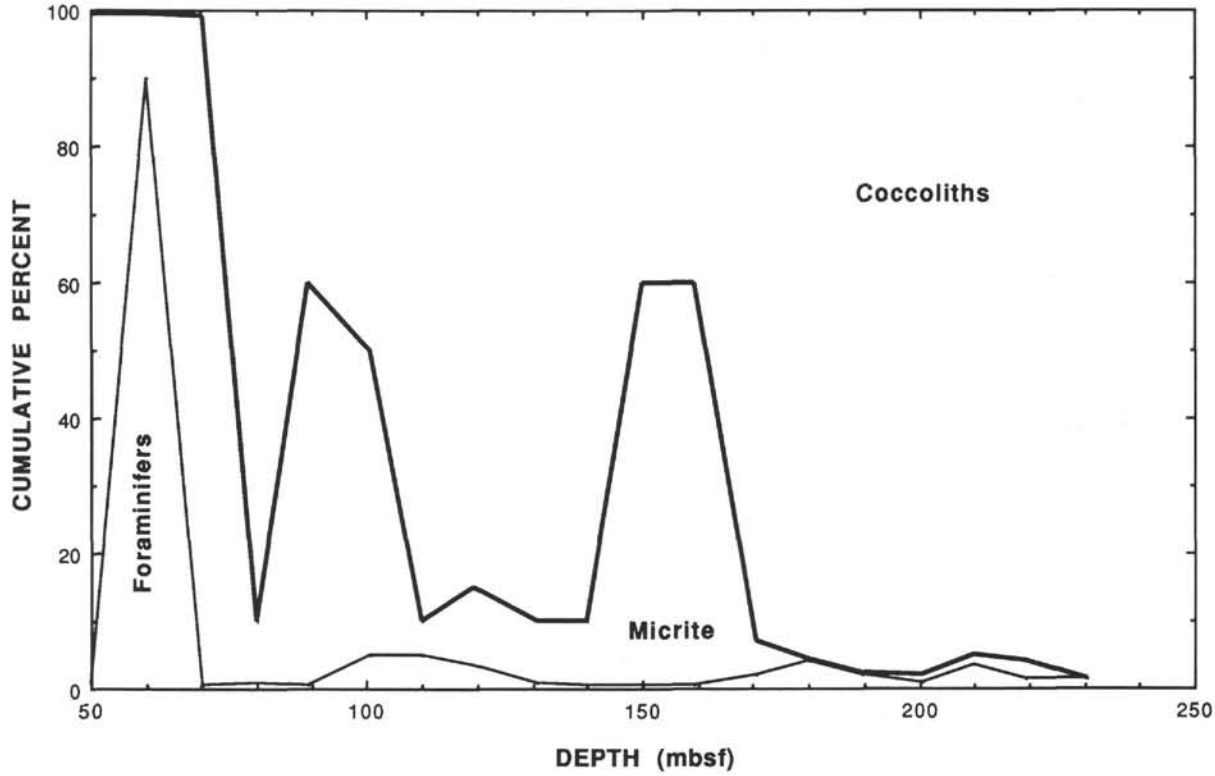

Figure 4. Random-settling slide analysis vs. depth.

downward increase that might be expected if diagenesis increased downhole.

DISCUSSION

This discussion will deal primarily with the large $\delta^{13}C$ shift at 2.6 Ma; it will also touch on some aspects of the large changes in $\delta^{13}C$ and $\delta^{18}O$ above 50 mbsf in the fine-fraction record.

Several possible causes for changes in the Site 704 fine-fraction isotope record exist:

1. diagenetic effects;
2. changes in the fine-fraction composition
   a. change in the nannofossil assemblage
   b. change in percent of micrite or of juvenile or broken planktonic or benthic foraminifers;
3. paleoceanographic change
   a. changes in upwelling and primary productivity of surface waters
   b. movement of the Antarctic Polar Front.

Table 4. Estimated fine-fraction composition from random-settling slide analysis, Hole 704A.

Core, section, interval (cm)	Depth (mbsf)	Foraminifers (%)	Calcareous nannofossils (%)	Micrite (%)
6H-4, 20	49.90	0.5	0.5	99
7H-4, 91	60.11	89.5	0.5	10
7H-4, 91	60.11	89.5	0.5	10
8H-4, 140	70.10	0.5	1	98.5
9H-5, 21	79.91	1	90	9
10H-5, 20	89.40	0.5	40	59.5
10H-5, 20	89.40	0.5	40	59.5
11H-6, 21	100.41	5	50	45
11H-6, 21	100.41	5	50	45
12H-6, 21	109.91	5	90	5
13H-6, 21	119.41	4	86	10
15H-1, 21	130.91	1	90	9
15H-1, 21	130.91	1	90	9
15H-1, 21	130.91	1	90	9
15H-7, 21	139.91	0.5	89.5	10
17X-1, 21	149.91	0.5	40	59.5
18X-1, 21	159.41	0.5	40	59.5
19X-2, 21	170.41	2	93	5
20X-2, 21	179.91	4	95.5	0.5
20X-2, 21	179.91	4	95.5	0.5
21X-2, 46	189.66	2	97.5	0.5
21X-2, 46	189.66	2	97.5	0.5
22X-3, 21	200.41	3.5	95	1.5
23X-3, 21	209.91	3.5	95	1.5
24X-3, 21	219.41	1.5	94	4.5
25X-4, 21	230.41	1.5	98.5	0

Diagenetic Effects

Initial examination of the preservation of the fine fraction found that slight etching of nannofossils occurs above Core 114-704B-10H (82.7–92.2 mbsf), and progressive overgrowth by secondary calcite below (Shipboard Scientific Party, 1988). We wish to determine whether this etching and overgrowth may have affected fine-fraction isotopic composition.

One indicator of a diagenetic overprint on isotopic composition would be for the isotopic composition of the fine fraction and/or planktonic foraminifers to follow that of the benthic foraminifers. Comparison of $\delta^{18}O$ records deeper than about 223 mbsf (5.0 Ma) (Fig. 5) shows that $\delta^{18}O$ of the fine fraction and of the benthic foraminifers are nearly the same, but that $\delta^{18}O$ of *Neogloboquadrina pachyderma* averages 0.5‰ to 1.0‰ lighter. Inspection of the carbon isotopic records (Fig. 6) reveals that fine-fraction and benthic foraminiferal $\delta^{13}C$ average about the same value in the interval from 170 to 58.5 mbsf (2.7–1.2 Ma), although $\delta^{18}O$ seems uncorrelated.

Diagenesis commonly affects $\delta^{18}O$ through exchange with pore waters or bottom waters. However, it rarely affects $\delta^{13}C$ in Cenozoic sediments because relatively little carbon is present in bottom waters or pore waters compared to that contained in carbonate on the seafloor or in sediments (Garrison, 1981). Therefore, we consider it unlikely that fine-fraction carbonate $\delta^{13}C$ would have been affected by diagenesis in the 170–58.5 mbsf interval without also affecting $\delta^{18}O$. In the 223–289.66 mbsf interval we suggest that although $\delta^{18}O$ values of the fine fraction may have been affected by diagenesis, $\delta^{13}C$ values have not.

Effects of Fine-Fraction Composition

Because a large shift in $\delta^{13}C$ occurs at 170–160 mbsf (Fig. 6), it is conceivable that the shift was caused by the change in fine-fraction composition at this point. This may well have had an effect, but it should also be noted that when the fine-fraction returns to close to the previous bulk composition in the 150–140 mbsf interval, the $\delta^{13}C$ values do not return to the values from below 170 mbsf nor do the compositional changes correlate to significant isotopic changes (Fig. 7). This argues against fine-fraction composition alone controlling isotopic composition. Because of the paucity of analyses in the Gauss, immediately below 170 mbsf, it is difficult to say how the covariance between $\delta^{13}C$ and $\delta^{18}O$ changes, but the shift in $\delta^{13}C$ is easily seen in examination of records from sediments above and below the Gauss/Matuyama boundary.

Paleoceanographic Change

The final possible cause of the shift in carbon isotopic values is a change in paleoceanographic conditions. Two interpretations of the decrease in $\delta^{13}C$ of fine-fraction carbonate along these lines are possible:

1. Decreased primary productivity leading to enrichment in ^{12}C in surface waters.
2. A northward shift in the position of the Antarctic Polar Front, causing an increase in upwelling rates.

Decreased primary productivity would allow ^{12}C to accumulate in surface waters, decreasing $\delta^{13}C$ instead of being preferentially extracted by plants. However, a decrease in primary productivity is not really a viable interpretation. Although carbonate content falls from an average of 72.7% to 42.7%, sedimentation rates increase significantly above the Gauss/Matuyama boundary, from an average of 22.3 m/m.y. to 3.3 times that, 73.0 m/m.y. Assuming that sediment densities remain constant, this would imply that accumulation rates of carbonate after the Gauss/Matuyama boundary increased by $3.3 \times (42.7/72.7) = 1.94$ times the pre-boundary value. Inspection of the sediments shows instead that lithologies change to become more biosiliceous-rich slightly below the boundary, at 178 mbsf (2.99 Ma) (Shipboard Scientific Party, 1988). This implies increased biosiliceous productivity as well. The increased sedimentation rate thus appears to be due to an increase in productivity of overlying waters, of both siliceous and calcareous components (Hodell and Ciesielski, 1990).

If a paleoceanographic change did lead to a change in $\delta^{13}C$ of total CO_2, that change probably was a northward shift in the position of the Polar Front. This would explain several features seen in the Site 704 sediments. Increased upwelling at the site would lead to increased productivity and therefore to an increased sedimentation rate. Second, the $\delta^{13}C$ of surface water would decrease. Third, as productivity increased, more organic carbon would be deposited on the ocean floor, which might help explain the simultaneous decrease seen in $\delta^{13}C$ of benthic foraminifers (but see Hodell and Ciesielski, this volume, whose alternate interpretation suggests a change in deep-water $\delta^{13}C$, a more likely explanation).

Several investigations have identified a trend of northward movement of the Polar Front from at least 2.9 to 1.9 Ma. Ciesielski and Weaver (1983) documented a northward shift in the position of the Polar Front over DSDP Site 514 (latitude 46°03′S) on the Falkland Plateau at 2.7–2.6 Ma, after which oscillations across the site occurred to at least 0.7 Ma. They based their findings on changes in radiolarian assemblages. Ciesielski and Grinstead (1986) refined the study of Site 514 by applying factor analysis to the radiolarian assemblages. Their results indicate increasing importance of Antarctic forms from 2.94 to 2.68 Ma, suggesting a progressive northward movement of the APFZ. From 2.67 to 1.91 Ma the Polar Front remained north of Site 514. Westall and Fenner (this volume) interpreted diatom and lithostratigraphic data from Hole 704B to infer northward movement of the APFZ at 101.7 mbsf (0.94 or 1.78 Ma according to their age models, 1.94 Ma according to our model—see Hodell and Ciesielski, this volume, for discussion of age models). At this depth, they found a further increase in biosiliceous content and a decrease in calcareous content. We would suggest that our data document movement of the northern boundary of the APFZ over Site 704 at 2.47 Ma, increasing carbonate and bulk accumulation rates, and that the data of Westall and Fenner (this volume) document the movement of the southern edge over Site 704 at 1.94 Ma, decreasing carbonate content but keeping total sedimentation rates high.

An increase in upwelling or mixing does not address the question of why the *Neogloboquadrina pachyderma* record does not show a similar depletion in $\delta^{13}C$ and why there is a consequent change in the fine fraction/*N. pachyderma* $\delta^{13}C$ gradient. The gradient between $\delta^{13}C$ of *N. pachyderma* and the fine fraction changes as a result of the shift in $\delta^{13}C$. The $\delta^{13}C$ of *N. pachyderma* averages 0.58‰ from the base of the Gauss to the shift, and virtually the same (0.59‰) from the shift to the top of the Matuyama, whereas the average $\delta^{13}C$ of the fine fraction changes from 1.26‰ to −0.22‰, respectively, in these same intervals. This represents a change in the fine fraction/*N. pachyderma* $\delta^{13}C$ gradient from 0.68‰ to −0.81‰, a difference of 1.49‰.

N. pachyderma has been characterized as a deep-living species, depositing much of its calcite under near-isothermal conditions or below the thermocline (Srinivasan and Kennett, 1974; Reynolds and Thunell, 1986). This suggests that the fine fraction is recording $\delta^{13}C$ of shallower water, while *N. pachyderma* is recording $\delta^{13}C$ of deeper, less variable water masses. Fine-fraction $\delta^{13}C$ would then be affected by the rate of upwelling and thus the position of the APFZ, which would control the balance between productivity and upwelling rate. *N. pachyderma* $\delta^{13}C$ would only record the average $\delta^{13}C$ of the upwelling water, which may not be affected by the rate of upwelling.

Because both the fine fraction (Margolis et al., 1975; Goodney et al., 1980; Paull and Theirstein, 1987) and *N. pachyderma* (Williams et al., 1977; Kahn and Williams, 1981; Charles and Fairbanks, 1990) deposit their calcite out of equilibrium with seawater-ΣCO_2, it is difficult to interpret the meaning of this gradient change. Both groups produce lower $\delta^{13}C$ values than equilibrium. In the subantarctic, *N. pachyderma* is approximately 1.0‰ too low (Charles and Fairbanks, 1990); therefore, we can use this value as a correction factor. However, the fine fraction produces $\delta^{13}C$ with variable relationships to equilibrium calcite; it is always light, but the correction varies.

Whether an increase in the upwelling to primary productivity ratio caused by a shift in the position of the APFZ is

responsible for the change in $\delta^{13}C$ at 2.6 Ma, or whether it is due to compositional change in the fine fraction, is somewhat problematical. Assemblage changes did occur at this time; this, coupled with the lack of an equivalent change in $\delta^{13}C$ in *N. pachyderma,* supports the interpretation that a change in the fine-fraction composition is at least partly responsible for isotopic changes. On the other hand, changes in gross composition that are not reflected in $\delta^{13}C$ occurred at other times as well (see Fig. 4). In addition, the very fact that the fine-fraction composition does change slightly before the Gauss/Matuyama boundary is evidence for the existence of environmental control.

Within the Matuyama, from 168.72 mbsf (2.47 Ma) to about 90 mbsf (1.7 Ma), the $\delta^{13}C$ of the fine fraction and of *N. pachyderma* exhibit a rough covariance. This suggests that after the APFZ moved north of Site 704, upwelling was intense enough for the $\delta^{13}C$ of the upwelled water to control the $\delta^{13}C$ of both the fine fraction and *N. pachyderma*.

The very large amplitude variations in $\delta^{13}C$ and $\delta^{18}O$ in the upper 70 m (mostly Brunhes paleomagnetic Epoch) of Site 704 deserve some mention. However, their interpretation is made difficult by the fact that because of the disturbance in this section, our knowledge of the chronostratigraphy is poor. This section exhibits some of the most extreme covariance between $\delta^{13}C$ and $\delta^{18}O$ at the site (Fig. 3). Goodney et al. (1980) demonstrated that the fine fraction shows a high degree of covariance. Paull and Theirstein (1987) demonstrated that this covariance is not necessarily related to water properties but instead to assemblage changes and that the assemblage changes can also lead to large changes in isotopic composition. Large changes in fine-fraction composition begin at about 80 mbsf and continue to at least 50 mbsf (Fig. 4), and we feel that the most likely source for the large isotopic variations is these compositional changes. To investigate this possibility further, changes both in gross composition (foraminifers vs. calcareous nannofossils vs. micrite percentages) and in species composition need to be addressed in the future. Although we do not yet understand the complete meaning of these isotopic changes, it should be noted that the changes in fine-fraction composition that occur simultaneously with these isotopic changes suggest variations in paleoceanographic conditions that also should be investigated.

CONCLUSIONS

Isotopic analyses of the fine-fraction carbonate of ODP Site 704 have supplemented isotopic analyses of *Neogloboquadrina pachyderma* and benthic foraminifers. The fine-fraction analyses revealed a shift toward lighter $\delta^{13}C$ at 2.6 Ma, corresponding to (1) a large increase in the sedimentation rate in Site 704 and (2) a simultaneous, almost identical shift in $\delta^{13}C$ in the benthic foraminiferal record. The fine fraction is made up of many components, and it is difficult to determine the exact cause of this shift. We suggest that it may be due to one or a combination of the following causes:

1. Changes in the fine-fraction composition.
   a. Change in the nannofossil assemblage.
   b. Change in percent of juvenile or broken planktonic or benthic foraminifers.
2. Increased upwelling of ^{12}C-enriched deep water, caused by a shift in the position of the Antarctic Polar Front.

This shift is part of a progressive northward movement of the APFZ, begun at least by 2.94 Ma (Ciesielski and Grinstead, 1986) and lasting at least until 1.90 Ma (Westall and Fenner, this volume).

The shift in $\delta^{13}C$ at this time is not seen in the $\delta^{13}C$ record from *N. pachyderma*, for reasons that are not clear at this time. We suggest that the reason for this may be the deposition of fine-fraction calcite primarily in depleted surface water, which is more affected by changes in upwelling rates than at deeper water levels, where the foraminifer *N. pachyderma* secretes its test.

ACKNOWLEDGMENTS

We thank two anonymous reviewers for making substantial improvements to the manuscript and to our conclusions. One of the reviewers suggested the deep-living habitat of *N. pachyderma* as the reason for the lack of correlation between carbon isotope records of foraminiferal and fine-fraction carbonate. GAM, DAH, and DWM did the isotopic analyses and thank R. Cooke for sample preparation and general laboratory assistance. PFC produced the stratigraphic framework and assisted in the fine-fraction compositional analyses.

This work was supported by a University of Florida Graduate Council Fellowship to GAM, U.S. Science Program (USSAC) Grant 20114 and NSF Grant OCE-8858012 to DAH, USSAC Grant 20115 to PFC, and NSF Grant DPP-8717854 to both DAH and PFC.

REFERENCES

Anderson, T. F., and Cole, S. A., 1975. The stable isotope geochemistry of marine coccoliths: a preliminary comparison with planktonic Foraminifera. *J. Foraminiferal Res.*, 5:188–192.

Barrera, E., and Savin, S. M., 1987. Effect of sample preparation on the $\delta^{18}O$-value of fine-grained calcite. *Chem. Geol.*, 66:301–305.

Berggren, W. A., Kent, D. V., Flynn, J. J., and Van Couvering, J. A., 1985. Cenozoic geochronology. *Geol. Soc. Am. Bull.*, 96:1499–1510.

Charles, C. D., and Fairbanks, R. G., 1990. Glacial to interglacial changes in the isotopic gradients of Southern Ocean surface water. *In* Bleil, U., and Thiede, J. (Eds.), *Geologic History of the Polar Oceans: Arctic versus Antarctic:* NATO ASI Ser., 519–538.

Ciesielski, P. F., and Grinstead, G. P., 1986. Pliocene variations in the position of the Antarctic Convergence in the southwest Atlantic. *Paleoceanography*, 1:197–232.

Ciesielski, P. F., and Weaver, F. M., 1983. Neogene and Quaternary paleoenvironmental history of Deep Sea Drilling Project Leg 71 sediments, southwest Atlantic Ocean. *In* Ludwig, W. J., Krasheninnikov, V. A., et al., *Init. Repts. DSDP*, 71: Washington (U.S. Govt. Printing Office), 461–477.

Dudley, W. C., Blackwelder, P. L., Brand, L. E., and Duplessy, J. C., 1986. Stable isotopic composition of coccoliths. *Mar. Micropaleontol.*, 10:1–8.

Dudley, W. C., Duplessy, J. C., Blackwelder, P. L., Brand, L. E., and Guillard, R.R.L., 1980. Coccoliths in Pleistocene-Holocene nannofossil assemblages. *Nature*, 285:222–223.

Garrison, R., 1981. Diagenesis of ocean carbonate sediments: a review of the DSDP perspective. *In* Warme, J. E., Douglas, R. G., and Winterer, E. L. (Eds.), *The Deep Sea Drilling Project: A Decade of Progress*: Soc. Econ. Paleontol. Mineral. Spec. Publ., 32:181–207.

Goodney, D. E., Margolis, S. V., Dudley, W. C., Kroopnick, P., and Williams, D. F., 1980. Oxygen and carbon isotopes of Recent calcareous nannofossils as paleoceanographic indicators. *Mar. Micropaleont.*, 5:31–42.

Hailwood, E., 1989. The role of magnetostratigraphy in the development of geological time scales. *Paleoceanography*, 4:1–18.

Hodell, D. A., Benson, R. H., Kennett, J. P., and Rakic, K.E.B., 1989. Stable isotope stratigraphy of late Miocene–early Pliocene sequences in northwest Morocco: the Bou Regreg Section. *Paleoceanography*, 4:467–482

Hodell, D. A., and Ciesielski, P. F., 1990. Southern Ocean response to the onset of Northern Hemisphere glaciation at 2.4 Ma. *In* Bleil, U., and Thiede, J. (Eds.), *Geologic History of the Polar Oceans: Arctic versus Antarctic:* NATO ASI Ser., 707–728.

Kahn, M. I., and Williams, D. F., 1981. Oxygen and carbon isotopic composition of living planktonic foraminifers from the northeast Pacific Ocean. *Palaeogeogr., Palaeoclimatol., Palaeoecol.*, 33:47–69.

Keigwin, L. D., Jr., and Shackleton, N. J., 1980. Uppermost Miocene carbon isotope stratigraphy of a piston core in the equatorial Pacific. *Nature*, 284:613–614.

Knox, F., and McElroy, M. B., 1984. Changes in atmospheric CO_2: influence of the marine biota at high latitude. *J. Geophys. Res.*, 89:4629–4637.

Kroopnick, P., 1980. The distribution of ^{13}C in the Atlantic Ocean. *Earth Planet. Sci. Lett.*, 49:469–484.

_____, 1985. The distribution of ^{13}C of ΣCO_2 in the world oceans. *Deep-Sea Res., Part A*, 32:57–84.

Lutjeharms, J.R.E., 1985. Location of frontal systems between Africa and Antarctica: some preliminary results. *Deep-Sea Res., Part A*, 32:1499–1509.

Margolis, S. V., Kroopnick, P. M., Goodney, D. E., Dudley, W. C., and Mahoney, M. E., 1975. Oxygen and carbon isotopes from calcareous nannofossils as paleoceanographic indicators. *Science*, 189:555–557.

Matthews, R. K., and Poore, R. Z., 1980. Tertiary $\delta^{18}O$ record and glacio-eustatic sea-level fluctuations. *Geology*, 8:501–504.

Miller, K. G., and Fairbanks, R. G., 1983. Evidence for Oligocene–middle Miocene abyssal circulation changes in the western North Atlantic. *Nature*, 306:250–253.

Miller, K. G., Mountain, G. S., and Tucholke, B. E., 1985. Oligocene glacio-eustasy and erosion on the margins of the North Atlantic. *Geology*, 13:10–13.

Moore, T. C., 1973. Method of randomly distributing grains for microscopic examination. *J. Sediment. Petrol.*, 43:904–906.

Paull, C. K., and Thierstein, H. R., 1987. Stable isotopic fractionation among particles in quaternary coccolith-sized deep-sea sediments. *Paleoceanography*, 2:423–429.

Raymo, M. E., Ruddiman, W. F., Backman, J., Clement, B. M., and Martinson, D. G., 1989. Late Pliocene variation in Northern Hemisphere ice sheets and North Atlantic deep water circulation. *Paleoceanography*, 4:413–446.

Reynolds, L. A., and Thunell, R. C., 1986. Seasonal production and morphologic variation of *Neogloboquadrina pachyderma* (Ehrenberg) in the northeast Pacific. *Micropaleontology*, 32:1–18.

Ruddiman, W. F., Raymo, M., and McIntyre, A., 1986. Matuyama 41,000-year cycles: North Atlantic Ocean and Northern Hemisphere ice sheets. *Earth Planet. Sci. Lett.*, 80:117–129.

Ruddiman, W. F., Raymo, M. E., Martinson, D. G., Clement, B. M., and Backman, J., 1989. Pleistocene evolution: Northern Hemisphere ice sheets and North Atlantic Ocean. *Paleoceanography*, 4:353–412.

Shackleton, N. J., Backman, J., Zimmerman, H., Kent, D. V., Hall, M. A., Roberts, D. G., Schnitker, D., Baldauf, J., Desprairies, A., Homrighausen, R., Huddlestun, P., Keene, J. B., Kaltenback, A. J., Krumsiek, K.A.O., Morton, A. C., Murray, J. W., and Westberg-Smith, J., 1984. Oxygen isotope calibration of the onset of ice-rafting and history of glaciation in the North Atlantic region. *Nature*, 307:620–623.

Shackleton, N. J., and Kennett, J. P., 1975. Paleotemperature history of the Cenozoic and the initiation of Antarctic glaciation: oxygen and carbon isotope analyses in DSDP Sites 277, 279, and 281. *In* Kennett, J. P., Houtz, R. E., et al., *Init. Repts. DSDP*, 29: Washington (U.S. Govt. Printing Office), 743–755.

Shipboard Scientific Party, 1988. Site 704. *In* Ciesielski, P. F., Kristoffersen, Y., et al., *Proc. ODP, Init. Repts.*, 114: College Station, TX (Ocean Drilling Program), 621–795.

Srinivasan, M. S., and Kennett, J. P., 1974. Secondary calcification of the planktonic foraminifer *Neogloboquadrina pachyderma* as a climatic index. *Science*, 186:630–632.

Williams, D. F., Sommer, M. A., II, and Bender, M. L., 1977. Carbon isotopic compositions of Recent planktonic foraminifers of the Indian Ocean. *Earth Planet. Sci. Lett.*, 36:391–403.

Date of initial receipt: 12 April 1989
Date of acceptance: 17 November 1989
Ms 114B-152

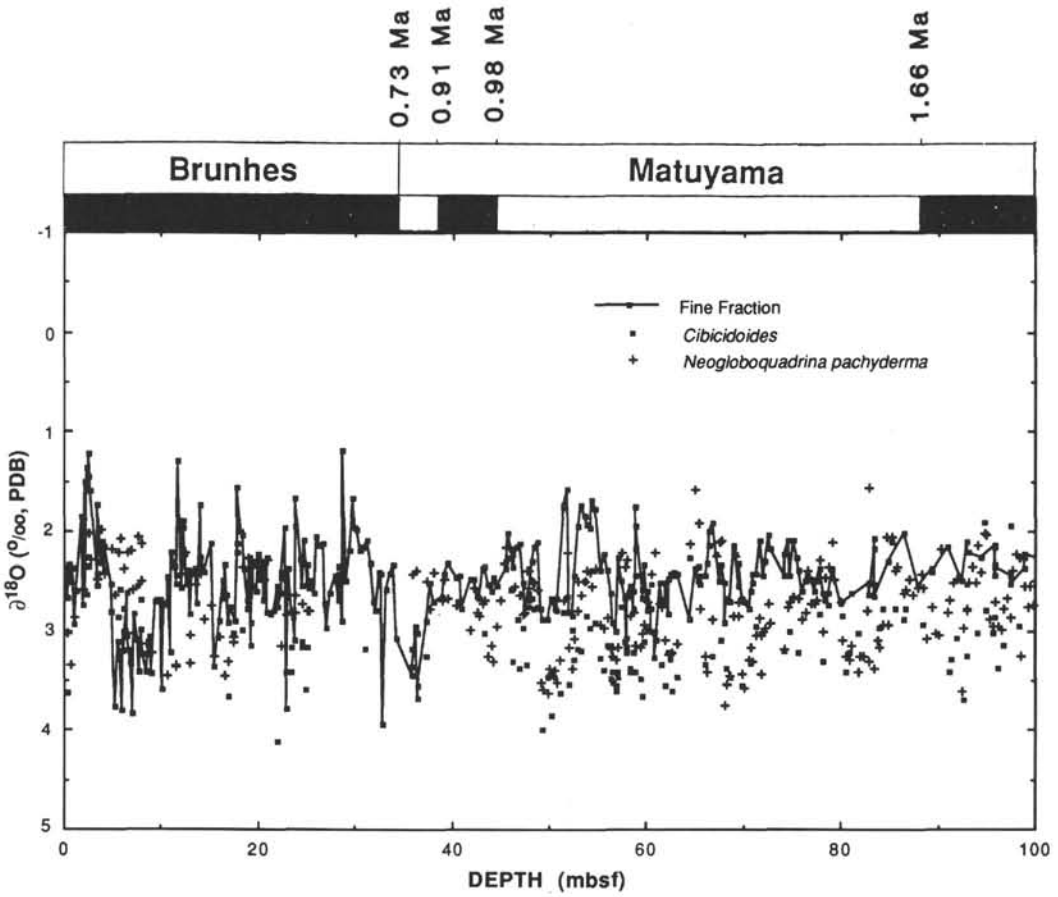

Figure 5. Comparison of $\delta^{18}O$ records from the fine-fraction and benthic and planktonic foraminifers vs. depth, 0–300 mbsf.

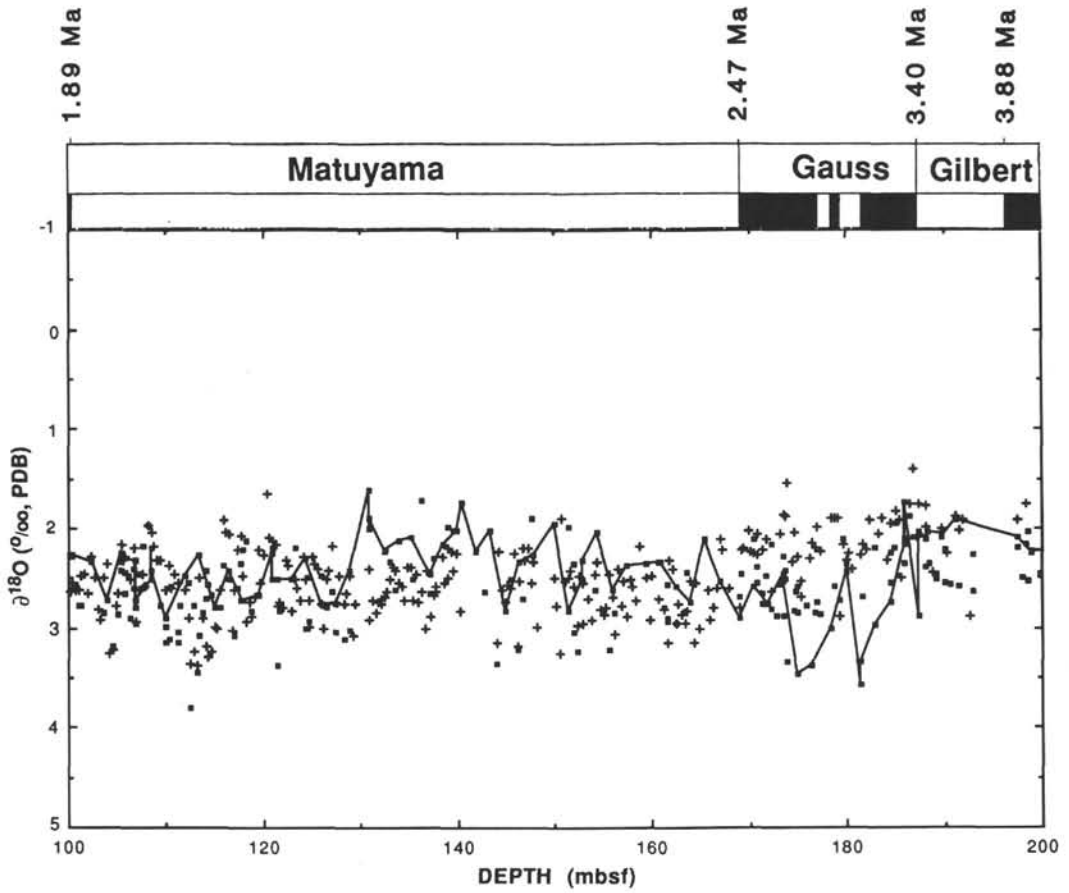

Figure 5 (continued).

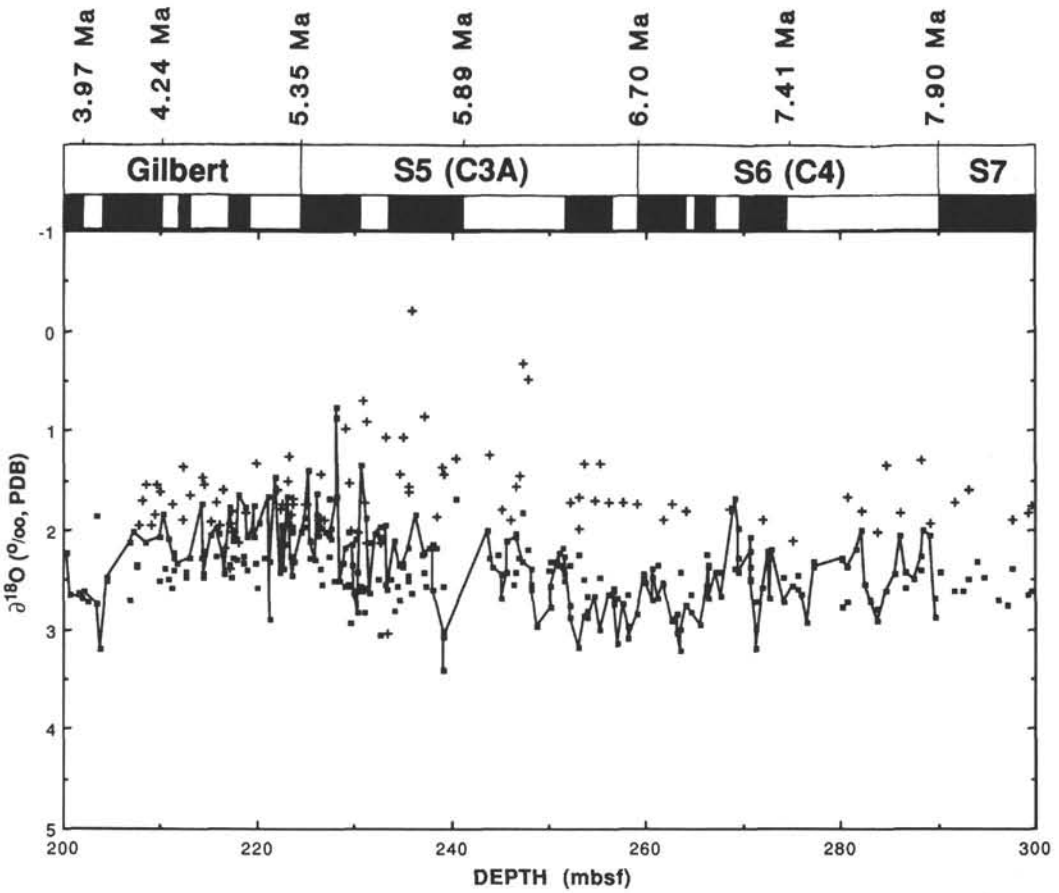

Figure 5 (continued).

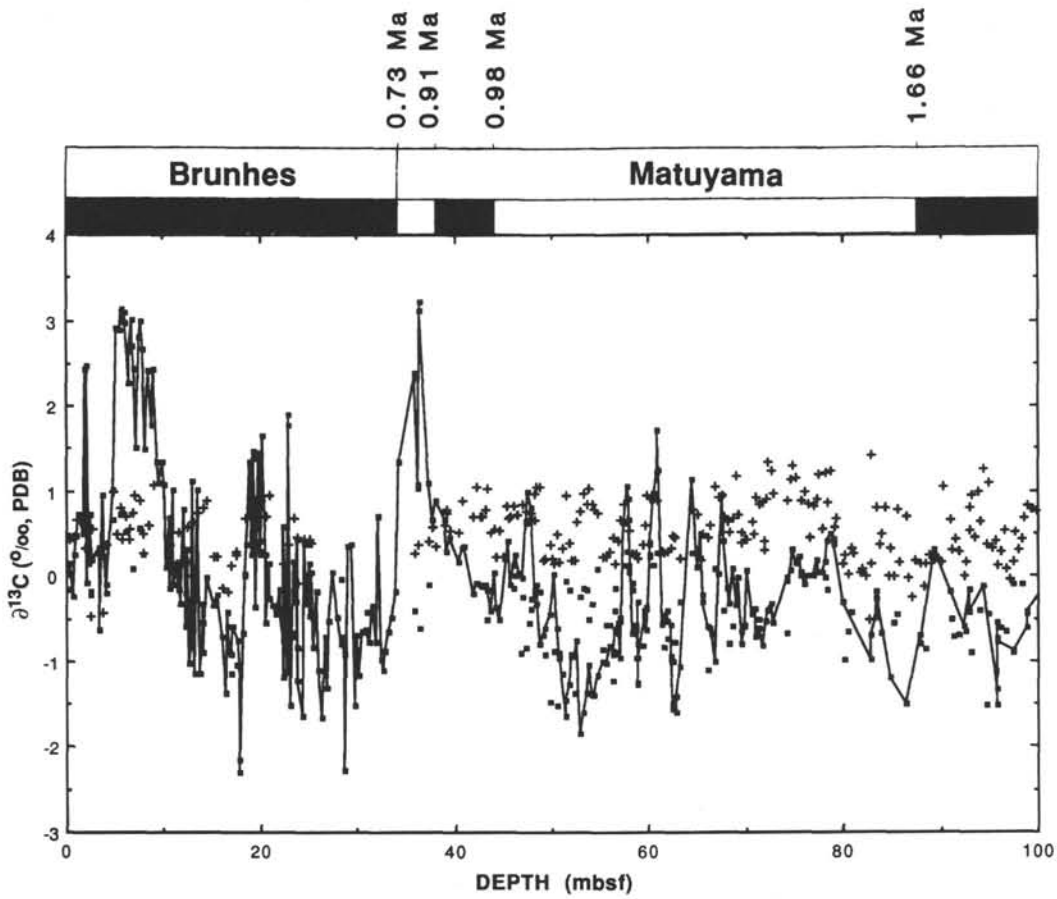

Figure 6. Comparison of $\delta^{13}C$ records from the fine-fraction and benthic and planktonic foraminifers vs. depth, 0–300 mbsf. Open boxes = fine-fraction analyses; crosses = *Neogloboquadrina pachyderma* analyses; solid boxes = *Cibicidoides* analyses.

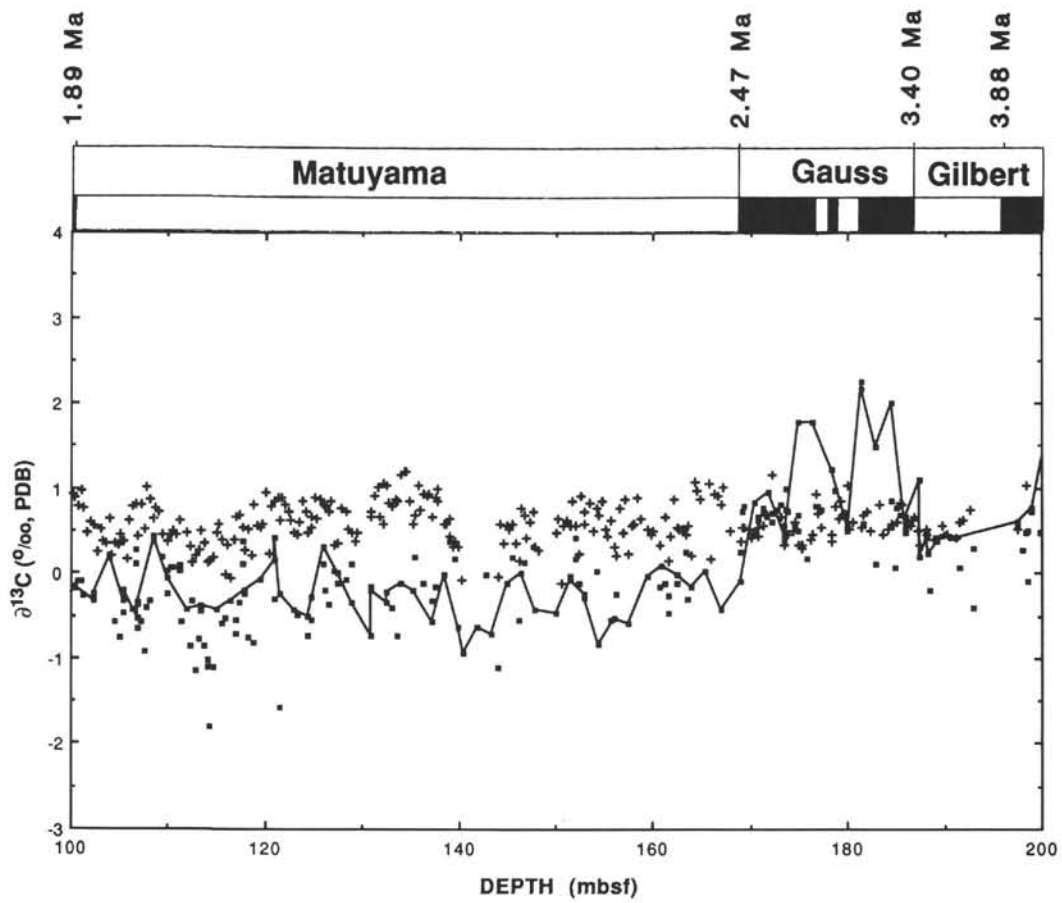

Figure 6 (continued).

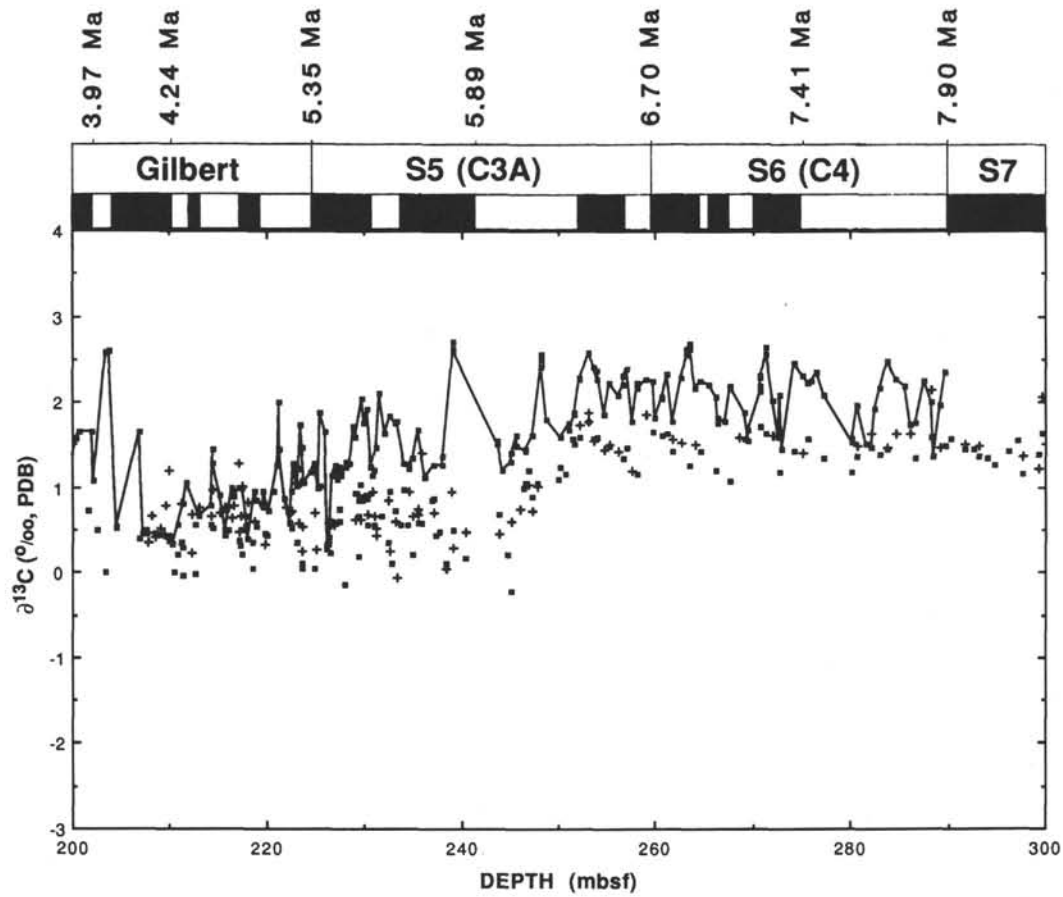

Figure 6 (continued).

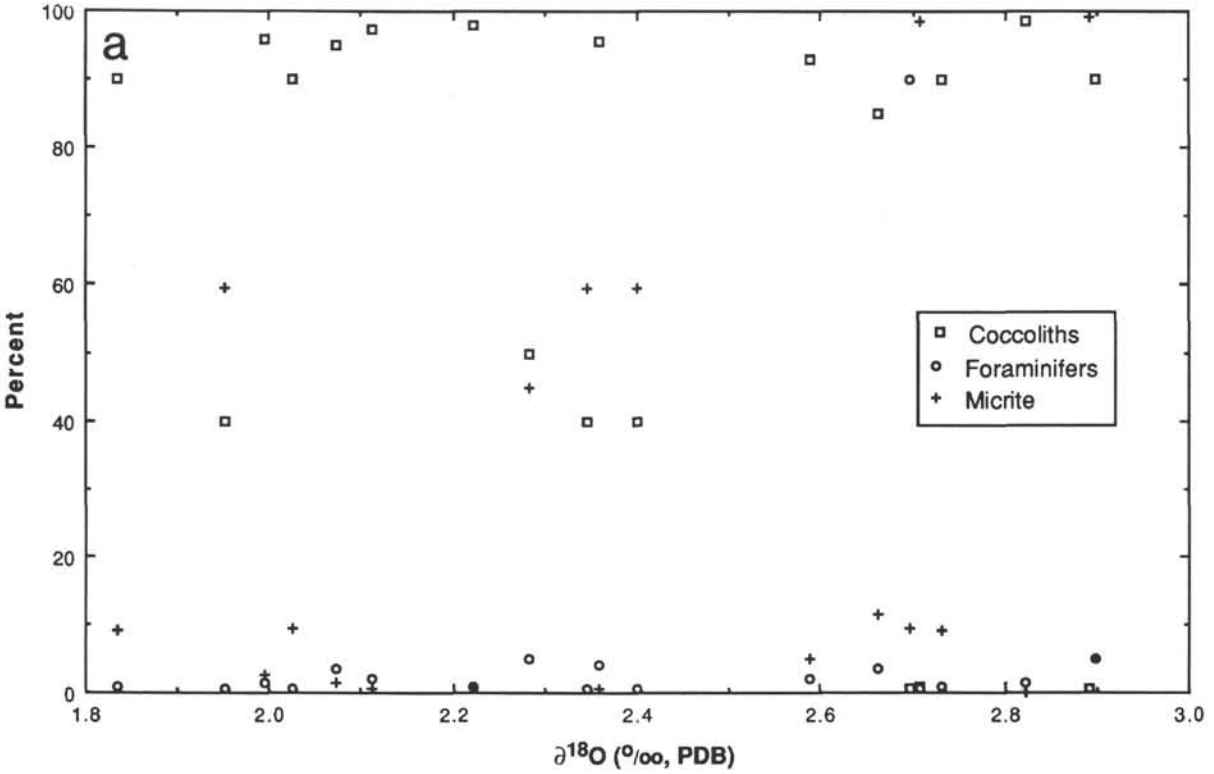

Figure 7. Fine-fraction composition vs. isotopes, Site 704. No correlation is visible between bulk fine-fraction composition and isotopic composition. **A.** $\delta^{18}O$. **B.** $\delta^{13}C$.

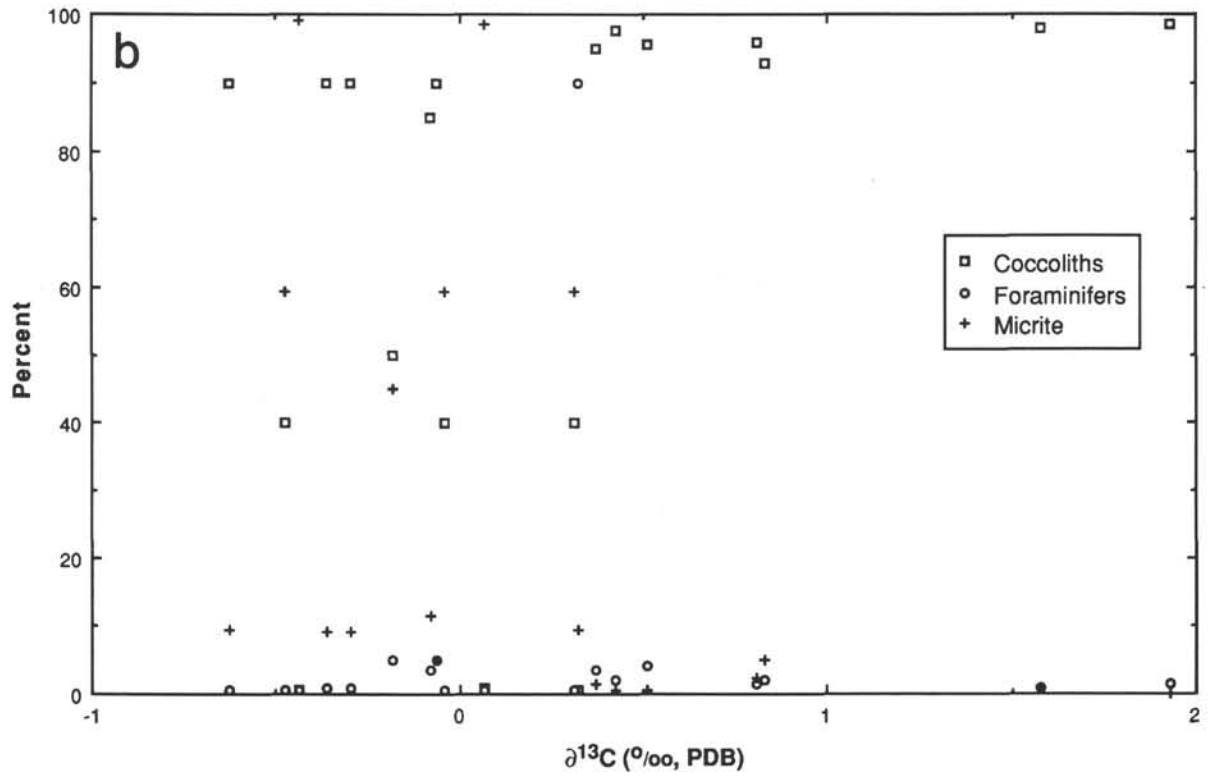

Figure 7 (continued).